

Luminosity Functions of XMM-LSS C1 Galaxy Clusters

Abdulmonem Alshino,^{1*} Habib Khosroshahi,² Trevor Ponman,¹ Jon Willis,³
Marguerite Pierre⁴, Florian Pacaud⁵ and Graham P. Smith¹

¹*School of Physics and Astronomy, The University of Birmingham, Birmingham B15 2TT, UK.*

²*School of Astronomy, Institute for Research in Fundamental Sciences (IPM), P. O. Box 19395-5531, Tehran, Iran.*

³*Department of Physics and Astronomy, University of Victoria, Elliot Building, 3800 Finnerty Road, Victoria, BC, V8P 1A1 Canada.*

⁴*DAPNIA/Sap CEA Saclay, 91191 Gif sur Yvette, France.*

⁵*Argelander-Institut für Astronomie, University of Bonn, Auf dem Hügel 71, 53121 Bonn, Germany.*

Accepted XXXX XXXX XX. Received XXXX XXXX XX; in original form XXXX XXXX XX

ABSTRACT

CFHTLS optical photometry has been used to study the galaxy luminosity functions of 14 X-ray selected clusters from the XMM-LSS survey. These are mostly groups and poor clusters, with masses (M_{500}) in the range 0.6 to $19 \times 10^{13} M_{\odot}$ and redshifts $0.05 \leq z \leq 0.61$. Hence these are some of the highest redshift X-ray selected groups to have been studied. Lower and upper colour cuts were used to determine cluster members. We derive individual luminosity functions (LFs) for all clusters as well as redshift-stacked and temperature-stacked LFs in three filters, g' , r' and z' , down to $M = -14.5$. All LFs were fitted by Schechter functions which constrained the faint-end slope, α , but did not always fit well to the bright end. Derived values of α ranged from -1.03 to as steep as -2.1 . We find no evidence for upturns at faint magnitudes. Evolution in α was apparent in all bands: it becomes shallower with increasing redshift; for example, in the z' band it flattened from -1.75 at low redshift to -1.22 in the redshift range $z = 0.43$ – 0.61 . Eight of our systems lie at $z \sim 0.3$, and we combine these to generate a galaxy LF in three colours for X-ray selected groups and poor clusters at redshift 0.3 . We find that at $z \sim 0.3$ α is steeper (-1.67) in the green (g') band than it is (-1.30) in the red (z') band. This colour trend disappears at low redshift, which we attribute to reddening of faint blue galaxies from $z \sim 0.3$ to $z \sim 0$. We also calculated the total optical luminosity and found it to correlate strongly with X-ray luminosity ($L_X \propto L_{OPT}^{2.1}$), and also with ICM temperature ($L_{OPT} \propto T^{1.62}$), consistent with expectations for self-similar clusters with constant mass-to-light ratio. We did not find any convincing correlation of Schechter parameters with mean cluster temperature.

Key words: galaxies: clusters: general - galaxies: evolution - galaxies: luminosity function - galaxies: structure.

1 INTRODUCTION

Most of our knowledge of galaxies is based on observations of the local universe, although distant universe observations have also provided a wealth of information. Statistical studies of galaxies at high redshift are mostly limited to rich galaxy clusters mainly due to observational limitations. Galaxy clusters are important cosmological environments where key galaxy transformation such as stripping and strangulation occur. However, in the hierarchical formation of structure rich clusters are the latest structures to be formed. Lower mass systems or galaxy groups may have been the place where galaxies experience a substantial degree of evolution through processes such as mergers and tidal interaction, as a re-

sult of the higher efficiency of these processes in the lower velocity dispersion environment of groups.

The Galaxy luminosity function (LF) – the number of galaxies per unit volume in the luminosity interval L to $L + dL$ – has been widely used to study the formation of galaxies and the evolution of galaxy populations with redshift. It is also an excellent statistical tool for describing how different environments influence the properties of galaxies.

Both the bright end (Bower et al. (2006), Naab et al. (2007)) and the faint end (Marzke et al. (1994), Khochfar et al. (2007)) of the LF have been the subject of in-depth studies, as they offer strong observational constraints for models of galaxy formation and evolution. While the bright end of the LF is affected by AGN feedback (Bower et al. (2006)), the faint-end slope is predominantly influenced by feedback from supernovae (Dekel et al. (1986)), and

* E-mail: alshino@star.sr.bham.ac.uk

provide a direct indicator of the significance of dwarf galaxies, which are expected to behave differently in rich and poor clusters. Multi-colour LFs, in particular, probe the history of the faint galaxy population, including its star formation history – see for example, Adami et al. (2007).

The vast majority of studies of the galaxy LF give faint-end slopes in the range ~ -1 to ~ -2 . Most of these have limited magnitude depth ($M > -16$) and recent deep studies are mostly confined to rich local clusters (See Table 1 in Popesso et al. (2005a) and Table A.1 in Boué et al. (2008) and references therein). These studies not only disagree on the value of the faint-end slope, but they also disagree on the exact form of it, as some studies (e.g. González et al. (2006)) found upturns; a single Schechter function was not an adequate fit to the faint end, and a double Schechter function was required to give a reasonable fit. The existence of these upturns is very sensitive to the method used to determine galaxy membership, with some approaches including spurious galaxies or excluding genuine cluster members due to their low surface brightness.

The evolution of the faint-end slope is hard to study, mainly because the number of faint galaxies detected decreases sharply with increasing redshift. Liu et al. (2008) found that the faint-end slope of a field galaxy population became shallower with increasing redshift (up to $z = 0.5$) for all galaxy spectral types. However, to account for the photometric redshift errors of the galaxies, they weighted the galaxies as probability-smoothed luminosity distribution at the redshift at which they were measured. This places an important caveat on the interpretation of their data, and hence on their results. On the other hand, simulations by Khochfar et al. (2007) show a measurable dependence of the faint-end slope of the galaxy luminosity function on redshift. However, most of this dependence is seen over a relatively large redshift range, $\Delta z \geq 2$. Furthermore, it is hard to discriminate galaxy environments in such studies.

X-ray surveys remain one of the most popular methods of finding galaxy systems. Due to the strong density dependence of X-ray emissivity, X-ray cluster selection is much less vulnerable to contamination along the line-of-sight than optical methods. The XMM-Large Scale Survey (XMM-LSS) (Pierre et al. (2004)), a contiguous X-ray survey, has a well-defined selection function which is used to produce a sample of galaxy groups to study their intracluster medium and galaxy properties at medium to high redshift. Pacaud et al. (2007) have presented a study of a sample of 29 galaxy systems from the XMM-LSS survey, drawn from an area of 5 deg^2 out to a redshift of $z = 1.05$. The cluster distribution peaks around $z = 0.3$ and $T = 1.5 \text{ keV}$, half of the objects being groups with a temperature below 2 keV .

In this paper, we use the XMM-LSS optical follow-up observations to study the evolution of the galaxy luminosity function in galaxy groups and poor clusters since $z \approx 0.6$. Given the observational biases – distant groups are more massive and hotter – we study whether the redshift dependencies are weaker or stronger when the intrinsic properties of the systems, for instance, intracluster medium temperature, are taken into account.

By using a deep ($m_g = 24$) optical survey of X-ray selected galaxy clusters up to redshift of $z = 0.61$, we aim in this paper to clarify the debate on the faint-end slope of the LFs of low-mass ($M_{500} \leq 20 \times 10^{13} M_\odot$) galaxy clusters (or groups), and to explore the existence of any dips, or upturns at the faint end, and to establish whether the slope shows trends with redshift or intracluster medium temperature. Comparison with previous results can help to elucidate the universality of galaxy cluster LFs. Furthermore, the scaling relation of total optical luminosity with temperature and

X-ray luminosity for our cluster sample can shed light on the mass-to-light ratios of low-mass systems when compared to rich clusters.

The paper is constructed as follows: In section 2, we describe the optical catalogue used to calculate the LFs. Then, we describe the data reduction and the method used to construct the colour-magnitude diagrams (CMD) and the subsequent LFs, and the technique adopted for the background subtraction. In section 3, we describe our results, starting with the individual cluster LFs, and then the redshift-stacked clusters and temperature-stacked clusters. In section 4, we discuss our results and compare them with other studies. Finally, in section 5, we summarise our conclusions.

Throughout this article, we adopt the cosmological parameters estimated by Spergel et al. (2007), namely: $H_0 = 73 \text{ km s}^{-1} \text{ Mpc}^{-1}$, $\Omega_m = 0.24$, $\Omega_\Lambda = 0.76$.

2 DATA

2.1 Observations

Optical photometry of the XMM-LSS survey was obtained from the Canada-France-Hawaii Telescope Wide Synoptic Legacy Survey¹, referred to as the CFHTLS Wide survey. Data were obtained in five passbands (u^* , g' , r' , i' , z') down to a nominal magnitude limit of $i' = 24.5$. Of the 19 deg^2 of CFHTLS Wide data available in the W1 survey area, 4 deg^2 overlap with the X-ray selected cluster catalogue presented by Pacaud et al. (2007). Hence our photometric data are drawn from four $1^\circ \times 1^\circ$ catalogues derived from the survey data.

The data used in this paper are based upon the reduction procedure outlined in Hoekstra et al. (2006). Source extraction and photometry were performed using SExtractor v2.5.0 (Bertin and Arnouts 1996). Zero point information for sources detected in the CFHTLS Wide field survey W1 area was extrapolated from common sources detected in the Sloan Digital Sky Survey equatorial patch which overlaps the southern edge of the W1 area.

XMM-LSS Class 1 (C1) clusters are a well-controlled X-ray selected and spectroscopically confirmed cluster sample. The criteria used to construct the sample guarantee negligible contamination by point-like sources. The observations of the clusters were performed in a homogeneous way (10-20 ks exposures). For full details of the C1 sample, see Pacaud et al. (2007). The main properties of the sample are shown in Table 1. Detailed information on the C1 selection process can be found in Pacaud et al. (2006). 17 out of the 29 XMM-LSS C1 clusters are covered by the CFHTLS Wide field survey. In this paper, we study the luminosity functions of 14 of these 17 clusters – dropping the three with the highest redshifts (clusters with XLSSC numbers 2, 29, and 1) because their photometric data is too poor to allow useful constraints to be obtained.

2.2 Analysis

Galaxies were detected by SExtractor (Bertin & Arnouts (1996)). Luminosity functions (LFs) were produced in three of the five CFHTLS (u^* , g' , r' , i' , z') filter bands, namely, g' , r' and z' . To determine the completeness of the LFs, we took into account the limiting apparent magnitude in each field. The completeness limits for each filter was determined using the apparent magnitude LFs of all data (down to the faintest magnitudes available) for each C1

¹ See <http://www.cfht.hawaii.edu/Science/CFHLS/>

cluster individually. Variations in seeing and exposure time across the CFHTLS fields used here are small, and it was found that for each filter there was a common completeness limit at which all LFs started to drop below the faint end power law slope. Note that the LF turn-up reported by some authors (see section 4.2), which could potentially introduce an error into this method for estimating completeness, falls beyond the faint limit of our LFs (e.g. at -16 in g' band), except in our three closest clusters, and hence cannot seriously bias our estimates of the completeness limits. The completeness threshold magnitudes for the three filters g' , r' and z' were found to be 24, 23.5 and 23, respectively. These values are also consistent with results based on comparison of the number counts per field to deeper data from the CFHTLS Deep Field and CCCP Megacam observations (Urquhart et al. (2009)).

Each entry in the catalogues is associated with a FLAG value which indicates the degree of reliability of the data. Flag is a short integer, and a value of 0 denotes good data. The more unreliable the data is, the higher the FLAG value becomes. We included all catalogue entries with $\text{FLAG} \leq 3$, which includes sources with very close and bright neighbours or some bad pixels and sources which are originally blended with other sources. This may admit some problematic galaxies but this is better than excluding many genuine cluster members, because many clusters contain significant number of blended sources. Factors that may raise the FLAG to > 3 include sources with saturated pixels, truncated sources, incomplete or corrupted data and sources with memory overflow during deblending or extraction. Catalogue entries with $\text{FLAG} > 3$ constitute only $\simeq 5\%$ of the total number of entries, and were all removed. Many of the removed entries are fainter than the threshold magnitude and hence would have been removed anyway.

Each entry in the catalogue also includes a stellarity class value, STAR, with values ranging from 0 to 1. The lower its value, the more likely the detected object is a galaxy. Data points with different STAR values were checked by IRAF and their radial profiles were examined to see if they matched the typical profile of a star or a galaxy. Typically, objects with $\text{STAR} > 0.85$ were found to be stars, whilst those with < 0.85 were galaxies. Therefore, only catalogue entries with STAR values of 0.85 or less were included when constructing the LFs.

Spectral temperatures of the XMM-LSS clusters, and the resulting values of R_{500} (which allow for the evolution in critical density with redshift), were measured by the Saclay team (Pacaud et al. (2007)). To construct colour-magnitude diagrams, we selected all galaxies within a circle of radius, $R^* = 1.5 \times R_{500}$ of the clusters. This radius limit, R^* , represents an estimate of R_{200} . Colour-magnitude diagrams were produced for all 14 clusters for colour bands: g' , r' and z' . The factor, 1.5 does not have a large effect on the fitted parameters of the Schechter function; we compared the results of $1.0 \times R_{500}$ to $1.8 \times R_{500}$ and found that the faint-end slope, α , was only changed within its 1σ errors.

The CMD was used to colour select galaxies which might be cluster members, hence reducing the background due to interlopers. The colours used for this were $u_2^* - g_2^*$ versus $g_{\text{kron}}' - r_2'$ versus r_{kron}' , and $i_2' - z_2'$ versus z_{kron}' for the three filters respectively, where the subscript 2 refers to the 2 arcsec aperture used in the magnitude measurements. To define and select cluster members in the CMD, we defined upper and lower colour cuts and only galaxies between these two lines were used to produce the LF, as galaxies outside these limits were most likely not cluster members. To define these two colour cuts, we first defined the red sequence line in the CMD and then pushed this line up and down to allow for statistical errors, and for the likely range of galaxy colours.

To define the red sequence line, we first defined the slope and then its Y-intercept. We checked that the BCGs lay at the centre of the X-ray emission in all clusters, and then calculated the red sequence slope in each case by fitting a straight line to the bright galaxies in the CMD. Bright galaxies are defined as those with magnitude ranging from that of the brightest cluster galaxy, m_{BCG} , to a magnitude of $m_{\text{BCG}} + 3$, inclusive. We found that the slope of the red sequence line for the 14 C1 clusters showed a mild trend with redshift: it was steeper for high-redshift clusters. A similar trend was observed by Gilbank et al. (2008) and attributed to a deficit of faint red galaxies at high redshifts, consistent with the galactic downsizing picture.

We divided our cluster sample into two redshift ranges: low-redshift clusters ($z < 0.2$) and intermediate-redshift clusters ($0.2 \leq z \leq 0.61$). Clusters from each group share a common red sequence line slope with a small variation. The common slope for the low-redshift range was -0.007 and -0.025 for the second range. Instead of using a different red sequence slope for each cluster, we used the common slope of the redshift groups for all clusters belonging to that redshift group.

The Y-intercepts of the red sequence lines were different for each galaxy cluster and depended on the average colour of the bright galaxies as defined above. To fix the value of the intercept for each cluster, the red sequence line was normalised so as to pass through the point in the CMD which has a magnitude of $m_{\text{BCG}} + 1.5$ and colour equal to the average colours of the bright galaxies. This point and the value of the slope completes the definition of the red sequence line.

Both upper and lower colour cuts have the same slope as the red sequence line. In order to define the upper colour cut, we have to determine the upper (red) limit to the cluster red sequence. We took into account the statistical scatter of the colours of the faintest galaxies on the red sequence. These galaxies are defined as those inside a 1.0×0.1 (magnitude by colour units) box in the CMD centred on the faint end of the red sequence line (see figure 1). The size of this box was chosen to include the faintest galaxies most probably belonging to the red sequence after studying the CMD of the C1 sample. The expected scatter of these galaxies, σ , is calculated by averaging their colour errors, that is the Y-axis errors in the CMD. The upper colour cut, is then taken to be the red sequence line pushed upward by 2σ . By taking into account this scatter, we ensure that almost all genuine cluster red sequence galaxies should fall beneath the red cut, since the statistical error on the brighter galaxies will be smaller.

Similarly, the lower (blue) colour cut is the red sequence line pushed downward in the CMD. In this case, the shift has to account for both statistical scatter, and for the fact that late-type cluster galaxies are intrinsically bluer than red sequence galaxies. The shift was therefore taken to be $-(2\sigma + \Delta)$. Where Δ is the theoretical colour difference between ellipticals and spirals. This was estimated using a simple model which calculates what colour late-type galaxies would have when redshifted by different amounts, as described in King & Ellis (1985). Δ is a function of redshift only and the redshift of the galaxy cluster was used to determine its value. This method of estimating Δ ignores any intrinsic evolution in the colour offset between red and blue cluster galaxies. However, the detailed COMBO-17 study of Bell et al. (2004) (see their Figure 1) shows that the colour difference between blue and red sequence cluster galaxies changes little over the redshift range (0-0.7) spanned by our clusters. Figure 1 shows an example of our use of colour cuts for selection of cluster galaxies.

Of course, background and foreground galaxies will still con-

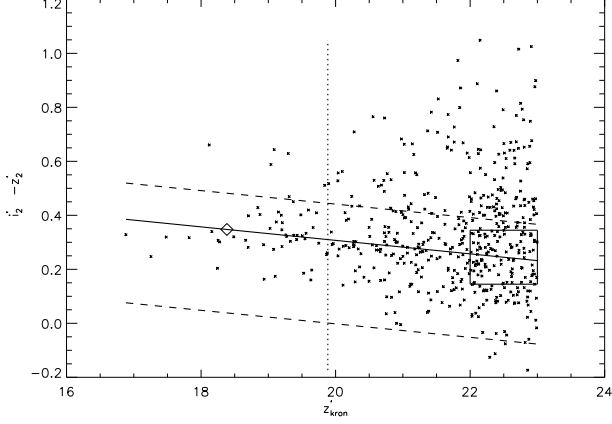


Figure 1. Colour-magnitude diagram of cluster 25 (redshift=0.26). All galaxies (crosses) on the left of the vertical dotted line are the bright galaxies with magnitude $\leq m_{\text{BCG}} + 3$. The red sequence line (the solid line) is defined by the point (diamond) with magnitude of $m_{\text{BCG}} + 1.5$ and colour equal to the average colours of all bright galaxies and by the slope of -0.025 . The statistical scatter, σ , is estimated by the average colour errors of the galaxies within the 1.0×0.1 box on the faint end of the red sequence line. In the case of cluster 25, $\sigma = 0.07$. The dashed lines are the upper and lower colour cuts. The upper colour cut is the red sequence line pushed upward by 2σ and the lower colour cut is the red sequence line pushed downward by $2\sigma + \Delta$, where $\Delta = 0.175$ for redshift of 0.26. See text for definition of Δ .

taminate the sample after the colour cut has been applied, and this contamination must be estimated and removed statistically. For this purpose we used all data in the catalogue to which a given galaxy cluster belonged. In addition to simple Poisson fluctuations, uncertainties in removing background and foreground galaxies arise from large scale structure. To quantify the extra fluctuations arising from this, we proceeded as follows. The whole catalogue $1^\circ \times 1^\circ$ area was divided into smaller blocks with areas comparable to that of the cluster in question. Any of these blocks covered mostly (60% or more, by area) by a galaxy cluster, were considered to be dominated by a cluster and hence were discarded from the background calculation. Blocks covered by clusters to an extent less than 60%, were not discarded but the portion covered by the R^* circle of any galaxy cluster was removed, so the final blocks used have somewhat different areas.

For each background block, an LF was produced in just the same way as for the cluster itself. The same values of the upper and lower red sequence limits of the galaxy cluster in question, were applied to all its background block areas, so galaxies beyond those limits were removed. The application of colour cuts to both source and background fields reduces the noise level in both of them, and hence in the final background-subtracted LF.

We then divided each background block LF by its area, added them and normalised the resulting single LF to the area of the galaxy cluster in question. The error bars on the averaged background LF were calculated from the scatter of the individual block LFs contributing to it. This method of estimating the background has some advantages over the more conventional background estimation method using an outer annulus around the galaxy cluster, since it uses a large background region, and the error estimate allows for the variance arising from the large scale structure. Finally, for each cluster we subtracted its composite background LF from the cluster LF, and propagated the errors.

Apparent magnitudes were converted to absolute magnitudes, using the distance for each cluster, and applying K-corrections calculated from Table 3 (for Hubble type E) in Frei & Gunn (1994). The use of early-type K-corrections is common in cluster studies, and justified by the dominance of early-type galaxies in clusters. However, if there were a systematic trend in early-type fraction with magnitude, then this could lead to some distortion of the LF slope. To quantify the maximum possible effect, we note that, using the tables in Frei & Gunn (1994), the K-correction for Hubble type E at $z=0.6$ for z' is 0.37 while it is 0.05 for Hubble type Im). Assuming (very conservatively) a systematic change from a 100% early-type to 100% late-type population across the faint end slope of our LFs, the impact of a differential error of 0.3 magnitudes on our determination of α would still only amount to $\Delta\alpha \approx 0.04$, which is small compared to the trends in alpha which represent some of our main results. The tables in Frei & Gunn (1994) apply to SDSS filters, which differ slightly from the corresponding MegaCam filters. The resulting differences in K-corrections are much smaller than the differences between early-type and late-type galaxies (about 0.03 at $z=0.1$ and 0.06 at $z=0.6$), and will have negligible effect on our derived LF slopes.

Finally, the data were binned into bins of width 0.5 magnitude (experiments showed that this bin size was a good choice in terms of fit quality and parameter confidence regions), and the resulting LFs were then fitted by a Schechter function model (Schechter (1976)),

$$\phi(M)dM = 0.4 \ln(10) \phi^* e^{-X} X^{1+\alpha} dM,$$

where $X = 10^{-0.4(M-M^*)}$, M^* is the characteristic magnitude, ϕ^* is the characteristic number density and α is the faint-end slope, Lin et al. (1996). Contour plots of the 1σ , 2σ and 3σ confidence levels of α and M^* were also produced. The errors in the text and tables refer to the 1σ errors. We also calculated the total optical luminosity L_{OPT} of each cluster by integrating the fitted Schechter function from $5 \times M^*$ to -16 .

In addition to single LFs for each galaxy cluster in our sample, we produced stacked luminosity functions. The radius used to determine the volume is the R^* of the cluster. Before stacking different clusters together, to correct for the evolution in the critical density of the universe, we multiply the LF by

$$\frac{\rho_c(z=0)}{\rho_c(z=z_{cl})},$$

where z is the redshift, ρ_c is the critical density of the universe, a function of z , and z_{cl} is the redshift of the cluster. This correction is necessary for high-redshift clusters if stacked with low-redshift clusters to scale the galaxy density in each cluster to the density at redshift=0. The faintest magnitude bin is not necessarily the same for each cluster and to account for this, we divided the total number of galaxies in each magnitude bin by the summed volume of galaxy clusters that contributed to that bin only. The stacked LFs should enable us to study the evolution of the LF with redshift and to explore any differences between clusters of different temperature.

3 RESULTS

3.1 Individual cluster luminosity functions

The fitted values of the three Schechter parameters α and M^* and L_{OPT} of the individual C1 clusters are presented in Table 2. The LF plots with the associated 1σ , 2σ and 3σ contours in the $M^*-\alpha$

XLSSC number	R.A. (J2000)	Dec (J2000)	Redshift	T (keV)	L_X $10^{43} \text{ erg s}^{-2}$	r_{500} (Mpc)
11	36.54	-4.97	0.05	0.64	0.11	0.29
21	36.23	-5.13	0.08	0.68	0.11	0.3
41	36.38	-4.24	0.14	1.34	2.4	0.44
25	36.35	-4.68	0.26	2.0	4.6	0.53
44	36.14	-4.23	0.26	1.3	1.2	0.4
22	36.92	-4.86	0.29	1.7	6.2	0.47
27	37.01	-4.85	0.29	2.8	4.8	0.65
8	36.34	-3.8	0.3	1.3	1.2	0.4
13	36.86	-4.54	0.31	1.0	1.3	0.34
40	35.52	-4.55	0.32	1.6	1.6	0.44
18	36.01	-5.09	0.32	2.0	1.3	0.52
6	35.44	-3.77	0.43	4.8	60.3	0.84
49	35.99	-4.59	0.49	2.2	4.3	0.49
1	36.24	-3.82	0.61	3.2	33.2	0.58
2	36.38	-3.92	0.77	2.8	19.6	0.49
29	36.02	-4.23	1.05	4.1	48.3	0.52
5	36.79	-4.3	1.05	3.7	17.1	0.49

Table 1. List of the 17 C1 galaxy clusters covered by CFHTLS optical survey and their properties sorted according to their redshifts (Pacaud et al. (2007)). The three highest redshift clusters (2, 29 and 2) though covered by the survey, were not included in our analysis because their data were too poor to yield useful fits.

plane for passbands r' and z' are shown in Figures A1 and B1 respectively. For some of the C1 clusters, the fitting failed to constrain some of the parameters, M^* in particular, due to poor statistics or the lack of any well-defined turnover in the LF at the bright end. For these clusters the LF and best fit are presented without any accompanying confidence contour plot. These LFs are placed at the bottom of the figures. For clusters with unconstrained M^* , L_{OPT} was also not constrained, because its value depends on both α and M^* . Therefore, we excluded these clusters in the part of the analysis related to L_{OPT} .

The average values of α for our sample of clusters are

$$-1.70 \pm 0.10, -1.64 \pm 0.04 \text{ and } -1.43 \pm 0.03$$

for the g' , r' and z' passbands respectively. The correlations between L_{OPT} , α and M^* and redshift, temperature (T) and the X-ray luminosity (L_X) taken from Pacaud et al. (2007), were tested using Pearson's correlation coefficient. These coefficients are computed from the ratio of the covariance of the tested variables, X and Y , to the square root of the product of the variances of these variables, i.e.

$$r = \frac{COV(X, Y)}{\sqrt{VAR(X) * VAR(Y)}}.$$

This correlation coefficient measures the linear correlation, if it is 1 or -1 then the two variables are perfectly positively or negatively linearly correlated, respectively. To compute the upper and lower 1σ errors on the correlation coefficient r , we used Fisher's Z transformation: $Z = \tan^{-1}r$. The strongest correlations found are those between L_{OPT} and T and between L_{OPT} and L_X , both of which are expected from the scaling relations of galaxy clusters. In our sample, they both have a correlation coefficient of at least 0.9, see Table 3.

Because higher redshift clusters are more difficult to detect than nearby ones, they will tend to be more massive and hence hotter than typical nearby clusters, see Figure 3 in Pacaud et al. (2007). This (*Malmquist*) selection effect is present in any deep cluster survey. To account for the $T - z$ correlation arising from this selection

effect in the C1 sample, for each correlation coefficient between a quantity and T or z , we have also calculated the partial correlation coefficient between the same two quantities, which attempts to remove any part of the correlation which arises due to the intrinsic trend in T with z within our sample. For this we used an Interactive Data Language (*IDL*) routine, *p_correlate.pro* to compute the partial correlation coefficient. This uses the following method, which to be concrete we explain using the example of the correlation between α and redshift. Let α and redshift z are the variables of primary interest, whilst temperature T is a third variable whose effects we wish to remove. First, the routine calculates the residuals after regressing α on T ; these are the parts of α that cannot be predicted by T . Likewise, it calculates the residuals after regressing z on T . Finally, the partial correlation coefficient between α and z , adjusted for T , is the correlation between these two sets of residuals.

The results of our correlation analysis for the unstacked clusters, are tabulated in the top section of Table 3. The correlation coefficients between the faint-end slope, α of the individual clusters and redshift are 0.44 ± 0.27 for the r' band and 0.54 ± 0.25 for the z' band. These coefficients, including the coefficient for the g' band, get stronger after the application of the partial analysis and the errors on the coefficients become smaller. This strongly suggests evolution of α with redshift in our sample. We will further scrutinise this possibility in the section of redshift-stacked clusters, because stacking LFs of clusters with similar redshifts should lower scatter in the data and provide a means to probe possible trends. M^* also shows a negative correlation with redshift and with temperature but these correlations become insignificant in a partial correlation analysis.

3.2 Global scaling relations

The relationships between the global cluster properties, L_{OPT} , L_X and T provide a probe of cluster self-similarity. L_{OPT} is strongly correlated to the temperature of our clusters – the correlation coefficients between L_{OPT} and T are 0.95 ± 0.06 , 0.96 ± 0.04 and 0.97 ± 0.03 for the g' , r' and z' bands respectively, whilst the partial

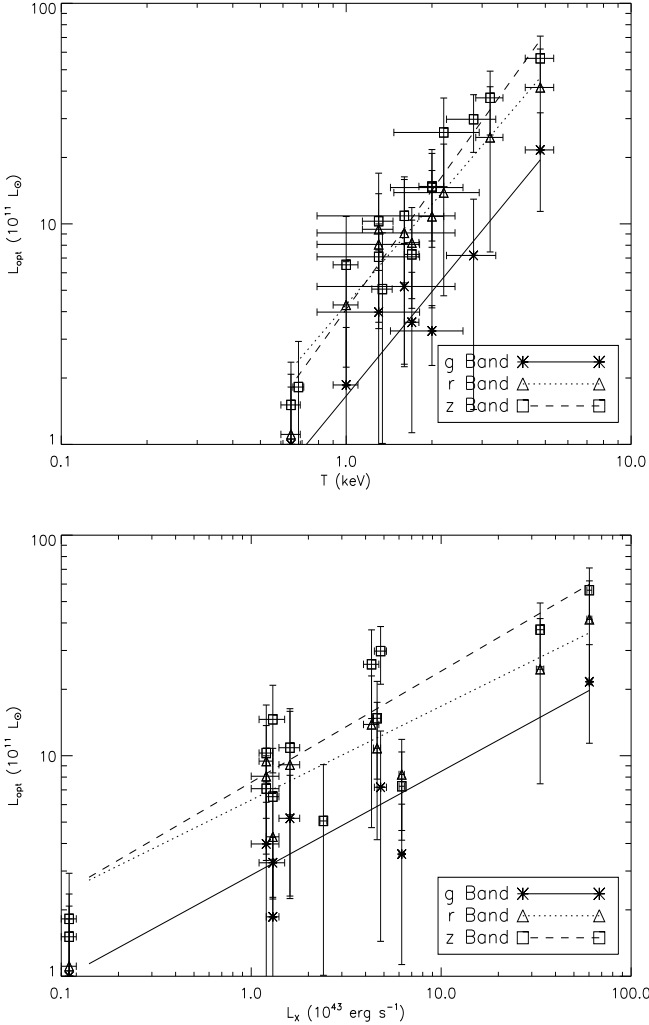


Figure 2. Correlation diagrams of L_{OPT} versus X-ray gas temperature, T (top panel) and L_{OPT} versus X-ray luminosity, L_X (bottom panel) of C1 clusters for passbands g' (stars), r' (triangles) and z' (squares). Clusters with unconstrained M^* and hence unconstrained L_{OPT} were excluded.

correlation coefficients for the same quantities, factoring out the effects of z , are 0.87 ± 0.16 , 0.89 ± 0.11 and 0.92 ± 0.06 , see third row in Table 3. The removal of the z effects has lowered the values of the coefficients but they are still high and significant. Correlation between L_{OPT} and L_X is also quite strong: 0.92 ± 0.11 (g' band), 0.93 ± 0.07 (r' band) and 0.90 ± 0.08 (z' band).

In Figure 2, we plot L_{OPT} versus T (top panel) and L_{OPT} versus L_X (bottom panel). We calculate the slopes for these plots using the *Fortran* package *ODRPACK* (Akritas et al. (1996)), which uses numerical orthogonal distance regression method to minimise perpendicular distances between points and the fitted line. One advantage of this is that the slope value will not change if the quantities in question switch axes. In addition, *ODRPACK* takes into account errors on both X-values and Y-values which are available for L_{OPT} , T and L_X .

The logarithmic slopes for the $L_{\text{OPT}} - T$ relation for the three filters g' , r' and z' , respectively are 1.57 ± 0.17 , 1.51 ± 0.17 and 1.79 ± 0.12 , giving an average value of 1.62 ± 0.11 . For the $L_{\text{OPT}} - L_X$ relation, the slopes are 0.47 ± 0.07 , $0.43 \pm$

0.08 and 0.50 ± 0.07 , and the average value is 0.47 ± 0.05 . Note that the slopes do not differ significantly for the three filters, except the slope of L_{OPT} versus T in the z' filter. Such relations between L_{OPT} on one hand, and L_X and the gas temperature on the other, are expected because richer and hence more luminous clusters have deeper gravitational potential wells which in turn raise the ICM temperature and its X-ray output by adiabatic compression and shocks generated by supersonic motion. We will discuss this further in Sec. 4.7.

The correlation coefficients between L_{OPT} and redshift are high (all above 0.8), but when the effects of temperature are removed they become insignificant in at least two of the filter set, therefore, this correlation is most likely due to selection effects, *Malmquist effect*, and does not reflect any genuine relationship between L_{OPT} and z . Correlations between α and M^* and T , z and L_X were also computed, but none of those showed significantly high values.

Following the above analysis of trends in the properties of individual clusters, we now perform a stacking analysis, grouping clusters first by redshift, and then by temperature. This provides LF of higher statistical quality, enabling the behaviour to be examined in greater detail.

3.3 Redshift-stacked clusters

The 14 C1 clusters span a redshift range 0.05 to 0.61. This range was divided into five redshift bins: 0.05-0.14, 0.26-0.26, 0.29-0.29, 0.30-0.32 and 0.43-0.61. The number of clusters in each bin ranges from two to four. The redshift ranges of these bins were chosen according to two criteria: first, the redshift range of the combined clusters was not too large, and second we required adequate data quality in each bin, to allow a well-constrained Schechter function fit. We kept the number of bins to at least five because a smaller number of bins increases the errors on the correlation coefficients. Plots of the redshift-stacked data with fitted Schechter functions for the three photometric bands are shown in Figures 10, 11 and 12, and results of the fits are given in Table 4.

The faint-end slope, α of the Schechter function of the stacked data shows an evolutionary trend, becoming less steep with increasing redshift. Three of the redshift bins (0.26-0.26, 0.29-0.29, 0.30-0.32) have very similar redshifts and in general the α values for these three bins agree within their errors.

The Pearson and partial correlation coefficients were calculated for α and z , see Table 3. The coefficients are high (≥ 0.88) but with relatively large errors, mainly due to the small number of bins. The partial correlation analysis lowered the values of the coefficients and enlarged the errors. Evidence for evolution in α is seen in all three bands, arising primarily from the fact that the faint-end slope is steeper ($\alpha = -1.75$ to -1.8) in the low z bin than in the higher redshift bins.

One obvious concern in probing evolutionary trends in the Schechter function fits is that the fitted magnitude range decreases systematically with redshift, due to the apparent magnitude limit of our data. A second effect which might bias α is that within a given redshift bin, the contributing clusters are probed down to different absolute magnitudes, according to their distance. Hence at the faint end, clusters may progressively drop out of the stacked LF. This is especially the case for the lowest and highest redshift bin, which are both much broader than the three bins at $z \approx 0.3$. To show the scale of this latter effect, we have drawn a vertical dotted line on each of the stacked LF plots (9, 10, 11, 12, 13, 14 and 15) to show the faintest magnitude to which *all* clusters in the bin contribute.

XLSSC number	g Band	r Band	z Band
α			
1	-1.94±0.23	-1.59±0.2	-1.06±0.17
6	-1.61±0.16	-1.7±0.09	-1.31±0.09
8	-1.53±0.37	-1.39±0.2	-1.15±0.16
11	-1.67±0.09	-1.8±0.05	-1.71±0.04
13	-1.63±0.63	-1.5±0.07	-1.51±0.08
18	-1.21±0.88	-1.76±0.13	-1.53±0.12
21	-2.01±0.11	-1.89±0.06	-1.77±0.06
22	-1.62±0.26	-1.19±0.19	-1.16±0.15
25	-2.1±0.12	-1.73±0.09	-1.57±0.08
27	-1.78±0.14	-1.85±0.12	-1.56±0.1
40	-1.03±0.3	-1.55±0.13	-1.27±0.09
41	-1.84±0.07	-1.86±0.09	-1.67±0.08
44	-1.75±0.12	-1.47±0.07	-1.44±0.09
49	-1.99±0.38	-1.65±0.16	-1.36±0.12
M^*			
1	-34.65±***	-23.7±0.91	-23.47±0.32
6	-20.96±0.43	-23.24±0.5	-22.98±0.23
8	-21.42±2.11	-21.79±0.83	-22.55±0.69
11	-20.61±1.5	-21.81±1.84	-21.13±0.73
13	-19.78±1.22	-22.19±0.37	-24.31±0.73
18	-19.66±1.43	-31.09±***	-22.23±0.41
21	-30.21±***	-29.02±***	-21.16±0.8
22	-20.26±0.84	-20.62±0.39	-22.15±0.5
25	-29.29±***	-22.66±0.78	-22.98±0.52
27	-22.22±1.32	-33.02±***	-23.52±0.76
40	-21.3±0.78	-22.95±0.96	-23.21±0.5
41	-30.57±***	-32.2±***	-23.38±1.5
44	-33.23±***	-22.79±0.53	-23.42±0.62
49	-31.66±***	-23.06±0.82	-23.72±0.46
$L_{OPT} 10^{11} L_{\odot}$			
1	57.51±***	24.66±17.2	37.27±11.98
6	21.64±10.25	41.53±20.52	56.29±14.72
8	3.98±3.63	3.07±1.92	7.09±3.74
11	1±0.82	1.11±0.97	1.51±0.85
13	1.86±1.53	12.93±4.75	23.17±12.84
18	1.27±0.99	107.34±***	14.61±6.25
21	0.94±***	4.19±***	1.82±1.11
22	3.58±2.45	4.22±1.64	7.27±3.13
25	10.95±***	10.81±6.65	14.78±6.95
27	7.19±5.75	42.62±***	14.81±8.72
40	5.2±2.95	10.1±6.79	12.87±5.47
41	12.99±***	12.21±***	5.06±4.05
44	95.01±***	9.45±4.25	13.28±6.7
49	17.41±***	13.86±9.14	25.97±11.23

Table 2. Results of the Schechter function fitting of the LFs of the 14 C1 galaxy clusters. For some clusters, the M^* values were not constrained by the fitting program and the errors of these unconstrained M^* are starred. Also, the errors of the corresponding L_{OPT} values are starred, since the computation of L_{OPT} depends on both α and M^* .

To the right (fainter side) of this line, one or more of the clusters in the redshift bin drop out of the stacked data.

To check whether the trend of α with redshift is robust against these two effects, we carried out tests on the stacked data, by progressively removing the faintest magnitude bin in the stacked LFs and re-fitting. In general, we found no significant change in the fitted values of α (which changed only within their errors), or in the

Quantities	g' Band P.C. Coeff.	r' Band P.C. Coeff.	z' Band P.C. Coeff.
Individual non-stacked C1 clusters			
L_{OPT}, L_X	0.92±0.11	0.93±0.07	0.90±0.08
L_{OPT}, T	0.95±0.06	0.96±0.04	0.97±0.03
L_{OPT}, T, z (Partial)	0.87±0.16	0.89±0.11	0.92±0.06
L_{OPT}, z	0.82±0.21	0.83±0.16	0.86±0.10
L_{OPT}, z, T (Partial)	0.28±0.44	0.36±0.36	0.61±0.22
α, L_X	-0.08±0.30	0.23±0.30	0.64±0.21
α, T	0.01±0.29	0.05±0.30	0.54±0.25
α, T, z (Partial)	0.00±0.29	-0.37±0.28	-0.17±0.30
α, z	0.01±0.29	0.44±0.27	0.54±0.25
α, z, T (Partial)	0.20±0.30	0.67±0.20	0.65±0.21
M^*, T	-0.32±0.43	-0.57±0.31	-0.48±0.26
M^*, T, z (Partial)	-0.47±0.41	-0.15±0.37	-0.02±0.29
M^*, z	-0.06±0.43	-0.57±0.31	-0.48±0.26
M^*, z, T (Partial)	0.25±0.44	0.00±0.36	0.00±0.29
Redshift-stacked			
α, z	0.97±0.10	0.88±0.29	0.89±0.29
α, z, T (Partial)	0.91±0.24	0.65±0.58	0.51±0.65
M^*, z	-0.86±0.33	-0.87±0.31	-0.71±0.53
M^*, z, T (Partial)	-0.21±0.67	-0.58±0.62	-0.33±0.68
Temperature-stacked			
α, T	0.10±0.64	0.31±0.68	0.75±0.49
α, T, z (Partial)	-0.44±0.67	-0.85±0.35	-0.45±0.67
M^*, T	-0.46±0.67	-0.26±0.67	0.67±0.56
M^*, T, z (Partial)	0.20±0.67	-0.46±0.67	0.25±0.67

Table 3. Pearson's correlation coefficients (P.C. Coeff.) of individual C1 clusters, redshift-stacked clusters and temperature-stacked clusters for the three-filter set (g' , r' , z'). 'X,Y,Z (Partial)' denotes partial correlation coefficient of quantities X and Y with effects of quantity Z removed, to be compared with the line directly above it, where correlation coefficient of the same quantities X and Y is presented without partial analysis.

α - z correlation when the LFs were truncated at the vertical dashed line, or when the LFs for all redshift bins were fitted to the same limiting absolute magnitude (which is set by the most distant systems). There was one exception to this. The three clusters in the highest redshift band (clusters 1, 6 and 49) all have α values (albeit with large errors) steeper than the shallow slope of -1.31 which fits to the stacked data in the g' band for this high redshift bin. As the faintest bins, to the right of the dashed line in the bottom plot of Figure 10, are progressively removed, the fitted slope steepens. Hence the flat slope of -1.31 must be regarded as unsafe, and the very high α - z correlation in g' band, given in Table 3, is probably overestimated. Rather, we have a situation in all three photometric bands, where the faint-end slope is steeper at $z < 0.2$ than it is at higher redshift.

To visualise the behaviour of the faint-end slope in terms of both redshift and colour, we plot the faint end of the fitted luminosity functions for the three bands in Figure 3 using green for g' band, red for r' band and black for z' band. For this plot, we have divided the sample into three redshift bins: low (0.05-0.14), intermediate (0.26-0.32) and high (0.43-0.61), denoted by different line styles. All LFs have been renormalised to have $\phi = 1$ at $M = -19.5$.

The Figure shows how the faint end slope steepens towards low z . It also illustrates colour trends in α . At low redshift (solid lines), the slopes are very similar (though the curves are separated

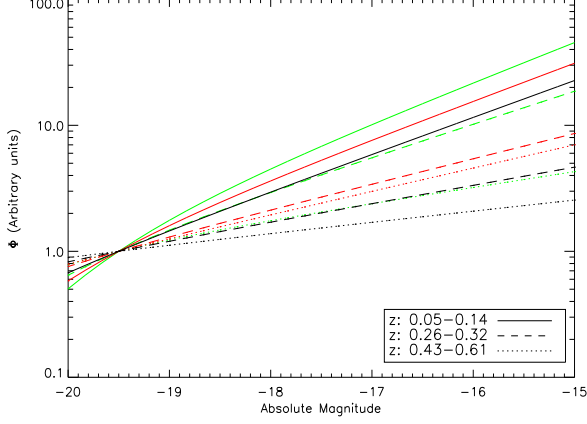


Figure 3. The faint end of the fitted LFs of the C1 sample grouped into three redshift bins: low (0.05-0.14, solid lines), intermediate (0.26-0.32, dashed lines) and high (0.43-0.61, dotted lines). Colours represent the filter bands: green for g' , red for r' and black for z' . All LFs were normalised to have $\phi = 1$ at $M = -19.5$ for easy comparison. The faint end slopes become shallower with increasing redshifts. Also, at intermediate redshift (dashed lines), the slope shows a trend with colour, becoming steeper towards the blue. This colour trend largely vanishes at low redshifts (solid lines).

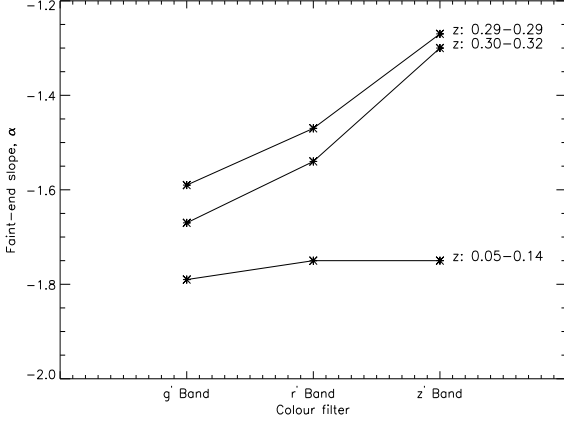


Figure 4. The faint-end slope of the fitted Schechter function in g' , r' and z' bands for local clusters with redshift 0.05 to 0.14 and for intermediate redshift ($0.29 \leq z \leq 0.32$) clusters.

due to their different values of M^*), whilst at intermediate redshift (dashed lines), the slope shows a strong trend with colour.

The values of α in Table 4 also show a trend with colour. The faint-end slope of z -stacked clusters becomes steeper as we move from z' (red side) band to g' (blue side). This trend is very obvious in the second, third and fourth redshift bins ($0.29 \leq z \leq 0.32$) and much less obvious and maybe absent (within the errors) in the first bin ($z \leq 0.14$), see Figure 4 in which we plotted the values of α for the three bands for the lower- and intermediate redshift bins. The increase in the faint-end slope of the Schechter function in the bluer bands means that at the faint side of the colour-magnitude diagram the blue galaxies outnumber red ones.

To explore this we produced K-corrected colour-magnitude diagram (Figure 5) of $g' - z'$ versus absolute r_{KRON} magnitude for $0.29 \leq z \leq 0.32$ (six clusters: 8, 13, 18, 22, 27 and 40) in which this trend is most obvious, and the same plot for the first redshift

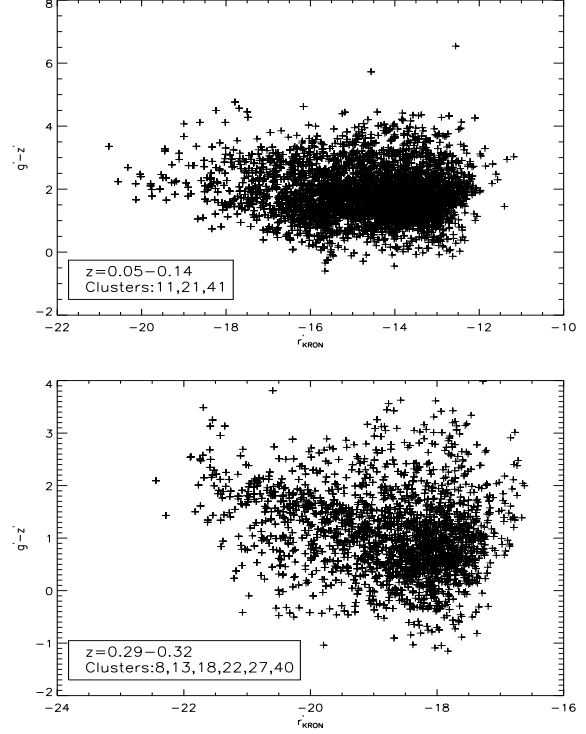


Figure 5. Colour-magnitude diagram: $g' - z'$ versus r' (K-corrected) for low-redshift ($z=0.05-0.14$) clusters and intermediate-redshift ($z=0.29-0.32$) clusters.

bin, $0.05 \leq z \leq 0.14$ in which no such trend is apparent. Figure 5 clearly demonstrate how the distribution of cluster galaxy colours changes from $z \sim 0$ to $z \sim 0.3$. In the g' band the evolution of α is much stronger, especially after removing the effects of the temperature (partial correlation). These trends in α show that the fraction of blue faint galaxies at $z \sim 0.3$ was larger than it is now, and suggests that these galaxies have reddened and moved

The Schechter function characteristic magnitude M^* in the redshift-stacked clusters showed a negative correlation with redshift. The correlation coefficients between M^* and redshift are high but less significant than those between α and redshift. However, when the partial calculations were carried out, these coefficients dropped and became consistent with zero. Hence the trend in M^* with z appears to be due to a selection effect: hotter clusters are more luminous, and so are more easily detected at high redshift, and these brighter clusters also tend to have brighter M^* (Zandivarez (2006)).

3.4 Luminosity functions of $z \sim 0.3$ clusters

Eight amongst the 14 C1 clusters, more than half of our sample, lie within the narrow redshift range 0.26 to 0.32. These clusters are representative of low-mass clusters at intermediate redshifts - a population which dominates the XMM-LSS cluster dataset. Stacking these clusters together provides the best available composite LF for X-ray selected poor clusters at $z \sim 0.3$, which should be valuable for future comparative studies. The LFs and their associated error contours are shown in Figures 6, 7 and 8.

These clusters range in temperature from 1.3 to 2.8 keV. Schechter fits give α values -1.66 ± 0.11 , -1.50 ± 0.05 and -1.36 ± 0.05 , and M^* values -21.07 ± 0.38 , -22.21 ± 0.22 and $-22.83 \pm$

0.17, for the g' , r' and z' bands respectively. Their faint-end slopes are shallower than the local clusters ($z \leq 0.14$) but steeper than higher-redshift ($z \geq 0.43$) ones. The colour trend of α is very obvious and seems to be a characteristic of $z \sim 0.3$ clusters compared to other clusters in other redshift bins, as mentioned above. Wilman et al. (2005a) studied a sample of poor clusters at redshift $z \sim 0.4$ selected from the CNOC2 galaxy redshift survey. Comparing this optically selected sample with nearby clusters, they found that the fraction of passive galaxies declines with redshift, which is consistent with our finding of larger population of faint blue galaxies at $z \sim 0.3$. However, these authors did not study the LF of their intermediate redshift groups.

In a recent study, Harsono & Propris (2009) presented composite LFs of six rich ($T \sim 7-9$ keV) clusters with redshifts ranging from 0.14 to 0.40 (averaging to 0.246) in the B,g,V,r,i and z bands. The LFs were well fitted by a single Schechter function with α values for g , r and z bands as follows: -1.31 ± 0.04 , -1.33 ± 0.03 and -1.45 ± 0.02 and the corresponding M^* values were -20.94 ± 0.17 , -21.95 ± 0.29 and -22.26 ± 0.30 . Their M^* values are in reasonable agreement with ours, but their slopes are shallower, and show no trend with colour. However, their data were limited to 20-40% of the area within r_{200} , and they suggest that the lack of any upturn in the slope at faint magnitudes may be related to this – the extra faint galaxies responsible for the upturn being associated with a population infalling into clusters. In contrast, our data extend to $1.5r_{500}$, which is approximately equal to r_{200} .

3.5 Temperature-stacked clusters

The 14 C1 clusters span a temperature range of 0.64 to 4.80 keV. This was divided into five subranges: 0.64-1.00, 1.30-1.34, 1.60-2.20, 2.80-3.20 and 4.80-4.80, using the same criteria, discussed above, which were used for stacking into redshift bins. The highest temperature bin consists of only one cluster because after removing the three high-redshift clusters (2,5,29), the temperature difference between the two highest temperature clusters was too large to stack them together, and the LF of the highest temperature cluster, cluster 6 ($T=4.80$ keV) was of sufficient quality that it provides useful constraints on its own. The second highest temperature bin consists of two clusters and the rest have at least three clusters.

The correlation coefficients of α with temperature are not high enough to establish any trend, especially when we take into consideration the reverse in sign of the coefficients after the partial correlation calculation, see Table 3. But in Table 4 the highest temperature bin contains only one cluster (cluster 6) and the other bins show some indication that α increases (slope decreases) with temperature, especially in bands r' and z' . Further investigation is needed to arrive at more conclusive results about the α trend with temperature. As to M^* , the stacked results do not show any trend with temperature. The LFs of the temperature stacked data are shown in Figures 13, 14 and 15.

Some previous studies (see for example, Miles et al. (2004)) found that galaxy clusters with low X-ray luminosity (comparable to the coolest clusters in our C1 sample) exhibit dips in their LFs. In our data, some of the temperature stacked LF plots (13, 14 and 15), especially those with high temperature (≥ 2.8 keV) showed signs of dips in the faint end of the LF. It can be hard to distinguish between scatter of the data points and a genuine dip in the LF.

To test the genuineness of these dips we fitted a Schechter function minus a Gaussian function defined by three parameters (central magnitude, width and depth) to these temperature stacked LFs. The two fits, with and without the Gaussian were statistically

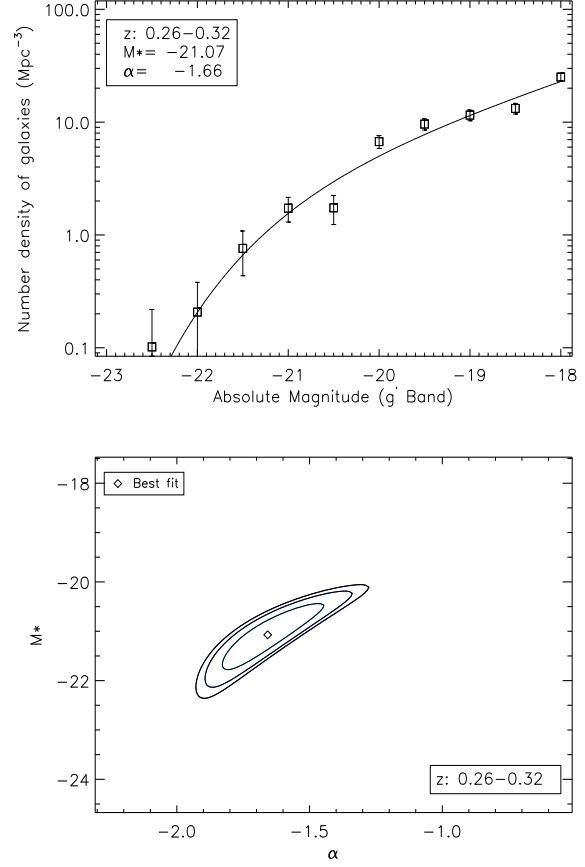


Figure 6. LFs of the 8 stacked C1 clusters with redshift 0.2 to 0.4 and their associated 1σ , 2σ and 3σ contours of confidence levels for α and M^* in the g' band.

compared using their χ^2 values, and an F-test applied to assess the significance of the improvement resulting from inclusion of the dip. In some cases the dip improved the fit at a confidence level of more than 90%. See, for example Figure 9.

However, careful examination of the stacked LF and the individual clusters LFs in these cases suggested that the dip is produced by the stacking of clusters with different faintest magnitude limits, rather than lying within the magnitude range shared by all the combined clusters. This was found to be true for all stacked LFs that showed a statistical improvement in fit on inclusion of a Gaussian dip. We therefore conclude that our data show no evidence for real dips in the optical LFs of the C1 clusters.

4 DISCUSSION

4.1 Faint-end slope of the luminosity function

In this work we have studied the LFs of the individual clusters in the C1 sample from XMM-LSS. A Schechter function provided a reasonable fit across most of the LF for most clusters, especially in the z' band. But the bright end was poorly-fitted for nearly half of the sample (6 out of 14) and M^* values were often not well constrained. The faint-end slope ranges are $-1.03 \leq \alpha \leq -2.1$, $-1.19 \leq \alpha \leq -1.89$ and $-1.06 \leq \alpha \leq -1.77$ with averages -1.70 ± 0.10 , -1.64 ± 0.04 and -1.43 ± 0.03 for the g' , r' and z'

Redshift-Stacked								
z-Range	Average T (keV)	Clusters- Stacked	α (g' Band)	α (r' Band)	α (z' Band)	M^* (g' Band)	M^* (r' Band)	M^* (z' Band)
0.05-0.14	0.89	11,21,41	-1.79 ± 0.05	-1.75 ± 0.03	-1.75 ± 0.02	-20.15 ± 0.51	-20.69 ± 0.48	-22.03 ± 0.54
0.26-0.26	1.65	25,44	-1.66 ± 0.10	-1.55 ± 0.07	-1.48 ± 0.07	-21.05 ± 0.36	-22.86 ± 0.48	-23.31 ± 0.46
0.29-0.29	2.25	22,27	-1.67 ± 0.13	-1.54 ± 0.10	-1.30 ± 0.10	-20.76 ± 0.47	-21.90 ± 0.46	-22.25 ± 0.35
0.30-0.32	1.48	8,13,18,40	-1.59 ± 0.22	-1.47 ± 0.07	-1.27 ± 0.07	-20.56 ± 0.58	-21.99 ± 0.25	-22.54 ± 0.21
0.43-0.61	3.40	1,6,49	-1.31 ± 0.09	-1.46 ± 0.08	-1.22 ± 0.06	-21.40 ± 0.26	-22.99 ± 0.31	-23.49 ± 0.18
Temperature-Stacked								
T-Range (keV)	Average z	Clusters- Stacked	α (g' Band)	α (r' Band)	α (z' Band)	M^* (g' Band)	M^* (r' Band)	M^* (z' Band)
0.64-1.00	0.15	11,13,21	-1.67 ± 0.05	-1.80 ± 0.02	-1.79 ± 0.02	-20.11 ± 0.45	-22.97 ± 0.58	-25.68 ± 2.13
1.30-1.34	0.23	8,41,44	-1.57 ± 0.05	-1.54 ± 0.05	-1.42 ± 0.04	-21.12 ± 0.30	-22.32 ± 0.31	-23.05 ± 0.28
1.60-2.20	0.34	18,22,25,40,49	-0.90 ± 0.10	-1.26 ± 0.05	-1.18 ± 0.04	-19.64 ± 0.20	-21.71 ± 0.18	-22.85 ± 0.17
2.80-3.20	0.45	1,27	-1.45 ± 0.08	-1.22 ± 0.07	-1.15 ± 0.05	-22.24 ± 0.44	-22.78 ± 0.28	-23.58 ± 0.20
4.80-4.80	0.43	6	-1.61 ± 0.16	-1.70 ± 0.09	-1.31 ± 0.09	-20.96 ± 0.43	-23.24 ± 0.50	-22.98 ± 0.23

Table 4. Results of the Schechter function fitting of the redshift-stacked and temperature-stacked clusters for the three-filter set (g' , r' , z').

passbands respectively. The mean faint-end slope, averaging over all the three filters, is $\alpha_{avg} = -1.59 \pm 0.05$.

Comparison of fitted Schechter parameters from different studies should take into account the passband, cluster redshift, and the procedure used in constructing the LF, including the methods used to determine the cluster membership and the background subtraction, since all of these factors may affect the results and therefore the accuracy of comparison.

Previous studies of galaxy cluster LFs have found a wide range for α , from $\alpha \sim -1$ (Paolillo et al. (2001)) to $\alpha \sim -2$ (Popesso et al. (2006)), but generally, LFs of clusters (both high-mass and low-mass systems) are found to have steeper slopes than field galaxy LFs, which usually span values $\alpha \sim -0.7$ (Lin et al. (1996)) to -1 (Loveday et al. (1995)). The values we obtain for α fall into the cluster LF range. The mass (M_{500}) range of the C1 clusters is $0.6-19 \times 10^{13} M_{\odot}$ (Pacaud et al. (2007)) and this puts the C1 sample in the lower-mass class of galaxy clusters (poor clusters and groups). This indicates that low-mass systems have almost the same range of faint-end LF slopes as more massive systems.

Moreover, González et al. (2006) studied LFs of galaxy clusters with a virial mass range $0.01 - 20 \times 10^{13} M_{\odot}$ and redshift $0.03 < z < 0.06$ and found slopes of $-1.9 < \alpha < -1.6$ at the faint end ($M_r \geq -18$). This is consistent with our result for clusters with comparable redshift; clusters 11 and 21, which have estimated masses of 0.6 and $0.9 \times 10^{13} M_{\odot}$ and redshifts 0.05 and 0.08 , show faint-end slopes of -1.80 ± 0.05 and -1.89 ± 0.06 in the r' band, with magnitude limits of -14.5 and -15 respectively.

The study of Popesso et al. (2005a) on X-ray selected rich clusters with $z \leq 0.25$ also gave a steep faint-end ($M_g \geq -16$) slope: $-2.1 \leq \alpha \leq -1.6$ in the SDSS g band. C1 clusters with redshifts ≤ 0.26 , namely clusters 11,21,25,41 and 44, have a g' band slope range of $-2.1 \leq \alpha \leq -1.67$, which agrees well with Popesso et al. (2005a). The redshift-stacked clusters with redshift $z \leq 0.32$ (the first four redshift bins) gave a slope range of $-1.79 \leq \alpha \leq -1.59$ in the g' band which is also consistent with Popesso et al. (2005a). The C1 clusters are low-mass systems, whilst the Popesso et al. (2005a) systems are rich clusters. The steep faint end slopes seen in both indicate a larger fraction

of dwarf galaxies in both groups and clusters, compared with the shallower LF slopes usually found in the field.

However, as is the case with richer clusters, the results from different studies of the luminosity function of group galaxies arrive at different results. For instance, Miles et al. (2004) derived a very flat ($\alpha \sim -1$) Schechter slope for X-ray bright groups – though they found a faint upturn in X-ray dim systems – and Zandivarez (2006) derived similarly low faint end slopes for SDSS groups. Miles et al. (2004) used photometric data of X-ray selected systems and used all galaxies with $B-R < 1.7$ from the regions outside a radius of R_{500} from the centre of the group as the background for subtraction, whilst Zandivarez (2006) used spectroscopic data for membership determination for their friends-of-friends selected clusters. Robotham et al. (2006) extracted LFs for 2PIGG groups, derived from the 2dF galaxy redshift survey, and obtained good fits with Schechter functions, with faint end slopes which increased from $\alpha \sim -1$ for red galaxies to $\alpha \sim -1.5$ for blue galaxies. These discrepancies in the faint-end slope from different studies could arise from a variety of causes: different cluster selection methods (X-ray selected clusters in our case), spectroscopic or photometric selection of cluster galaxies, different galaxy background subtraction techniques (see discussion in section 4.3), and possibly because different clusters have different faint-end slopes depending on their large-scale environment, which will affect the incidence of infalling galaxies.

4.2 The absence of the upturn in the faint end of LFs

Both Popesso et al. (2005a) and González et al. (2006) reported an upturn at the faint end of their stacked LF, and required a sum of two Schechter functions, rather than a single Schechter, to obtain reasonable fits. Popesso et al. (2005a) located the upturn at -16 in the g' band, and -18.5 in z' ; the upturn of González et al. (2006) was found at a similar magnitude: -18 in the r' band. In our sample, only the LFs for clusters 11,21 and 41 extend to the faint magnitudes in which Popesso et al. (2005a) and González et al. (2006) found their upturns. The composite LF for these systems is the first in the redshift-stacked LFs, see Figures 10, 11 and 12. Although our results agree with Popesso et al. (2005a) and González et al. (2006)

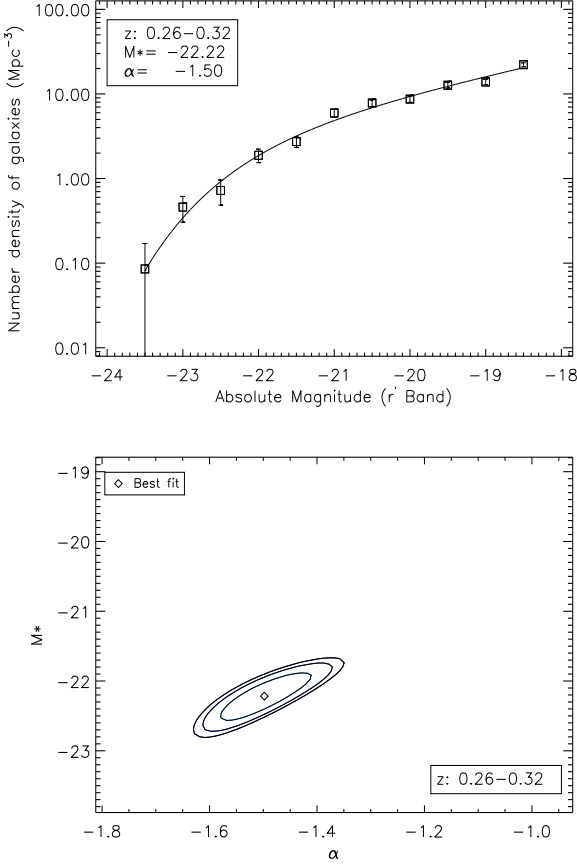


Figure 7. LFs of the 8 stacked C1 clusters with redshift 0.2 to 0.4 and their associated 1σ , 2σ and 3σ contours of confidence levels for α and M^* in the r' band.

regarding the steep values of the faint-end slope, we do not find any evidence for a departure from a simple power law at the faint end.

Other studies gave steep slopes at the faint end of cluster LFs but without evidence of sudden upturns, see for example Durret et al. (2002). Garilli et al. (1999) studied composite LFs of 65 clusters ranging in redshift from 0.05 to 0.25 and did not find upturns in their composite LFs. Popesso et al. (2005a) argued that Garilli et al. (1999) did not see this upturn in their stacked LF because they used a weighting for the individual LFs which depends strongly on the cluster magnitude limit, such that clusters with fainter magnitude limits, which contribute to the faint magnitude bins of the stacked LF, were heavily down-weighted. In our sample, only the LFs for clusters 11,21 and 41 extend to the faint magnitude region in which Popesso et al. (2005a) and González et al. (2006) found their upturn. The composite LF for these systems is the first in the redshift-stacked LFs, see Figures 10, 11 and 12. We did not apply any weighting method that depends on the magnitude limit and although faint-end slopes are steep in all three bands for the stacked LF of clusters 11,21 and 41, they lack any upturn at the locations found by Popesso et al. (2005a) and González et al. (2006). Furthermore, individual LFs of these three clusters do not show any obvious upturn in the faint-end part of the LF that can be distinguished from the scatter of the data relative to the fitted Schechter function.

Popesso et al. (2006) decomposed their LF by galaxy type and showed that the late-type galaxies LF was well fitted by a single

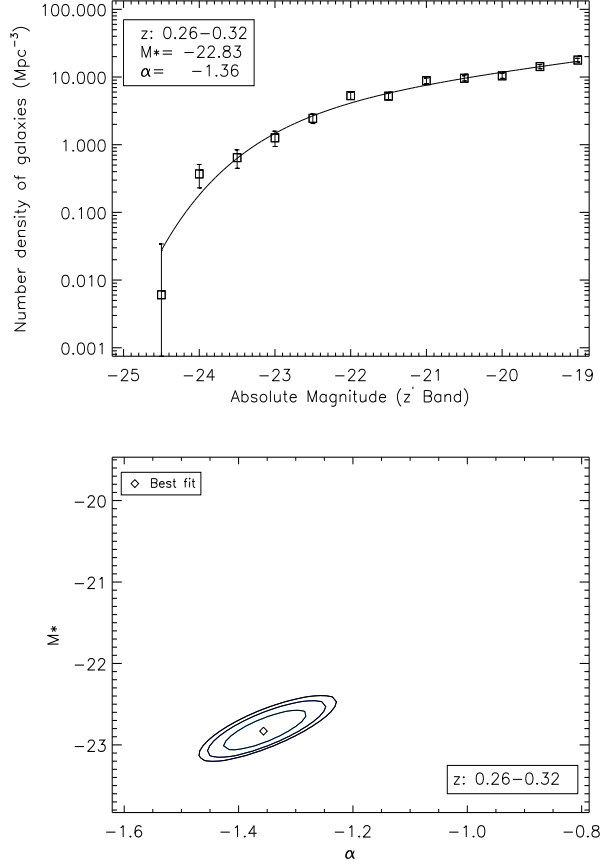


Figure 8. LFs of the 8 stacked C1 clusters with redshift 0.2 to 0.4 and their associated 1σ , 2σ and 3σ contours of confidence levels for α and M^* in the z' band.

Schechter function with a steep slope ($\alpha = 2.0$), while the early-type galaxies LF could not be fitted by a single Schechter function, and a composite of two Schechter functions was needed, such that the faint-end upturn of the global cluster LF was due to the early-type cluster galaxies. This suggests one way of reconciling our results with those of Popesso et al. (2006). If in our poorer clusters late-type galaxies outnumber early-types in the intermediate and faint magnitude ranges then the LF would be steep and without any upturns. This needs to be further investigated by studying the early-type and the late-type LF separately. Another possibility for the difference between our results and those of Popesso et al. (2006) lies in the techniques used to remove non-cluster galaxies, as we discuss in the next section.

4.3 Membership determination methods: Effects on α

The steepness of the faint end of the luminosity function reflects the number of dwarf galaxies within a cluster. Estimates of this number are very sensitive to the method used to estimate and remove the contribution of background and foreground galaxies before constructing the cluster luminosity function.

Rines & Geller (2008) compared methods of membership determination based on spectroscopic data and on photometric data (which we used) with regard to the resulting LF. They highlighted the advantages of spectroscopic identification of cluster members. Where automated photometric methods are used, they found, for

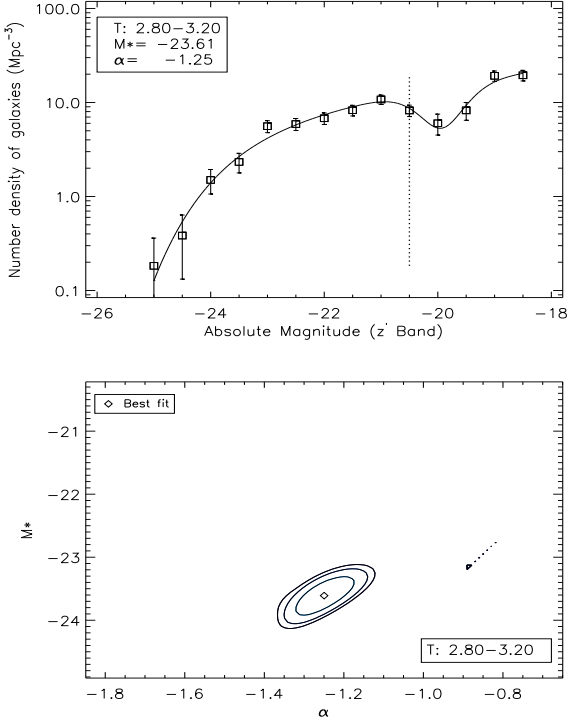


Figure 9. LF of the stacked clusters 1 and 27 (fourth temperature bin: $2.80 \leq T \leq 3.20$) with plot of the 1σ , 2σ and 3σ confidence contours in the α - M^* plane. The line is the fit of a Schechter function plus a Gaussian dip. The fitted dip position is -19.9 ± 0.1 (z' filter). The vertical dotted line marks the faintest magnitude at which both stacked clusters contribute.

example, that many large galaxies, especially those with low surface brightnesses, may be detected as many small separate objects, and warned that if these pieces of galaxies are not removed, they can produce an artificial excess of faint galaxies in cluster fields.

However, we have to emphasise that although spectroscopic data can give precise information on the cluster membership, their use to study cluster LFs is limited to relatively nearby clusters, since for higher-redshift clusters, spectroscopy is feasible only for the bright cluster galaxies. Boué et al. (2008) used deep multi-colour photometry to study the LF of A496, using colour selection to reduce contamination by red background galaxies, and did not find the large fraction of dwarf galaxies ($\alpha = 2.0$) inferred by some other authors, including Popesso et al. (2006). They suggested that this excess of dwarf galaxies in some studies might arise from inadequate removal of background, due to use of inadequate (or no) colour cuts. They claimed that the red sequence used by Popesso et al. (2006) was polluted by field galaxies because they used $u^* - r'$ vs i' in their CMD which Boué et al. (2008) showed was not efficient in rejecting background galaxies. In our study, we did not use $u^* - r'$ vs i' to define the colour cuts. Instead, we used $u^* - g'$ vs g' for the g' band, $g' - r'$ vs r' for the r' band and $i' - z'$ vs z' for the z' band. Moreover, our method of field LF subtraction is based on global background LF constructed by using the whole $1^\circ \times 1^\circ$ field of the cluster. Therefore, we don't see any obvious reason why we might have contaminated the red sequence with field galaxies in such away as to give a false steep faint-end slope.

4.4 Origin of the faint galaxies

Our results indicate that larger numbers of faint galaxies exist in cluster environments than in the field. It is not straightforward to understand this result, since various dynamical processes that can destroy dwarfs act more effectively in dense environments. Several ideas have been proposed to explain the excess of dwarfs in clusters. Babul & Rees (1992) argued that a primordial population of dwarf galaxies is preserved in high-pressure environments, whilst it fades away in low-pressure regions. Alternatively, dwarfs could be formed by galaxies that fell into clusters from the surrounding field and were morphologically transformed. The transformation mechanism could be tidal fragmentation or so-called harassment of infalling late-type spiral galaxies by the cluster potential or by close encounters (Moore et al. (1996)) or ram pressure stripping of dwarf irregular galaxies (e.g., van Zee et al. (2004)).

Boselli et al. (2008) showed that both simulations and observations are consistent regarding the scenario of recent accretion and transformation of low-luminosity star-forming galaxies in the Virgo cluster into quiescent dwarfs due to ram pressure gas stripping and galaxy starvation. They also showed that this process of transformation results in galaxies with structural and spectrophotometric properties similar to those of dwarf ellipticals. If the whole star-forming dwarf galaxy population dominating the faint end of the field luminosity function were accreted, it could be totally transformed by the cluster environment into dwarf ellipticals on timescales as short as 2 Gyr. These vigorous forces acting in cluster environments may explain the steepness of LFs faint-end slopes in nearby clusters.

4.5 The evolution of α

Our results show an evolutionary trend of the faint-end slope, α , in all bands used: g' , r' and z' . Liu et al. (2008) examined the faint-end slope of the V-band LF of *field* galaxies with redshifts $z < 0.5$ and found that it becomes shallower with increasing redshift: their α changed from -1.24 for the lowest redshift bin $0.02 \leq z < 0.1$ to -1.12 for the highest redshift bin $0.4 \leq z < 0.5$. In clusters, a recent study by Lu et al. (2009) of an optically selected cluster sample found steepening of the faint end with decreasing redshift since $z \sim 0.2$, and that the relative number of red-sequence dwarf galaxies had increased by a factor of ~ 3 .

It is possible that this LF slope trend with redshift is linked to the finding of Harsono & Propris (2007) that the 'upturn' in the LF faint end (i.e. the excess of galaxies above a single Schechter function) is found only in low redshift clusters. They attributed this to the recent infall of star-forming field galaxies or the whittling down of formerly more massive objects. The impact of recent infall of galaxies into clusters is also supported by the work of Lisker et al. (2007), who showed that dEs in the Virgo cluster fall into two major morphological subclasses: a) dEs with blue centres, thick disks or features reminiscent of late-type galaxies, such as spiral arms or bars; this class showed no central clustering, suggesting that they are an unrelaxed population formed from infalling galaxies. The second subclass is b) nucleated dEs – a fairly relaxed population of spheroidal galaxies indicating that they have resided in the cluster for a long time, or were formed along with it. Lisker et al. (2007) also pointed to other studies deriving similar results (see references therein), indicating that this subclassification is not specific to the Virgo cluster.

4.6 Colour trends

The faint-end slopes, α , of the redshift-stacked groups are steeper in bluer bands in almost all redshift bins. However, this trend is significant ($> 1\sigma$) only for the redshift range $0.29 \leq z \leq 0.32$. The redshift bin in which this effect seems to be absent is the first bin: $0.05 \leq z \leq 0.14$. This suggests that the fraction of faint blue galaxies in clusters of redshift $z \sim 0.3$ are higher than in local systems. Figure 5 further illustrates this and it also shows that these blue faint galaxies appear to have reddened and moved upwards in the colour-magnitude diagram. This is consistent with the findings of Wilman et al. (2005a) who compared the fractions of passive (red and quiescent) and blue star-forming galaxies in cluster at $0.3 \leq z \leq 0.55$ with nearby ($z \simeq 0$) clusters. They found that the fraction of passive galaxies declined strongly with redshift to at least $z \simeq 0.45$. These results are also consistent with the well-known Butcher-Oemler effect in clusters and support the idea that dense environments are responsible for galaxy transformation from blue to red because these trends are less obvious in field environments, see Wilman et al. (2005b).

Our result is also consistent with Yee et al. (2005) who studied the colours of galaxies as a function of luminosity and environment using the Red Sequence Cluster Survey and the SDSS. They found a higher incidence of faint to moderate luminosity galaxies in high density environments at $z > 0.2$ compared to lower redshifts and lower density environments. They interpreted this as arising from the shut-down of star formation in low mass galaxies within clusters at $z < 0.3$, in contrast to the situation in the field (c.f. Balogh et al. (2004)).

The fact that such transformations are observed in low-mass clusters like our C1 sample, as well as in richer clusters, favours mechanisms for suppression of star formation which operate in shallower potential wells, such as strangulation, tidal interactions and galaxy mergers, rather than ram pressure stripping, which is effective mostly in rich environments with high velocity dispersions.

4.7 Correlation between global properties of clusters

The optical luminosity is a good indicator of cluster richness, and hence should be closely related to cluster mass, velocity dispersion and temperature (Popesso et al. (2005b)). Assuming that cluster mass is directly proportional to the optical light (i.e. M/L_{OPT} is constant), that the ICM is in hydrostatic equilibrium and that X-ray luminosity L_X scales with gas temperature T as $L_X \propto T^3$ (Xue & Wu (2000)), it is expected that $L_{OPT} \propto T^{1.5}$, and that $L_{OPT} \propto L_X^{0.5}$.

Our scaling results for L_{OPT} with L_X and T mostly agree well with these expectations. For the $L_{OPT} - L_X$ relation, the logarithmic slopes are 0.47 ± 0.07 (g' band), 0.43 ± 0.08 (r' band) and 0.50 ± 0.07 (z' band). While for the $L_{OPT} - T$ relation, we have 1.57 ± 0.17 (g' band), 1.51 ± 0.17 (r' band) and 1.79 ± 0.12 (z' band).

Popesso et al. (2004) found 0.38 ± 0.02 for the $L_{OPT} - L_X$ relation and 1.12 ± 0.08 for the $L_{OPT} - T$ relation in the z SDSS band within a cluster radius of 0.5 Mpc (chosen to minimise the scatter in their scaling relations). The systems they used for their analysis, the RASS-SDSS sample, were X-ray selected, and ranged from low-mass systems of $10^{12.5} M_\odot$ to massive clusters of $10^{15} M_\odot$, over a redshift range from 0.002 to 0.45. Their logarithmic slope value for the $L_{OPT} - L_X$ relation is not inconsistent with our value (within the errors), however, their $L_{OPT} - T$ value is lower than ours. They attributed the departure of their re-

sults from the expected values to a breakdown in the assumption of constant mass-to-light ratio. More precisely, they argued that if the assumption of hydrostatic equilibrium was retained, their results would be in a good agreement with $M/L \propto L^{0.33 \pm 0.03}$, as found by Girardi et al. (2002). However, we note that extracting L_{OPT} within a fixed *metric* radius, will include a smaller fraction of the virial radius for higher mass clusters. Hence it should be no surprise if the $L_{OPT} - T$ relation is flattened below the expected slope of 1.5 for self-similar clusters. Using clusters from the RASS-SDSS sample, Popesso et al. (2005b) calculated L_{OPT} within r_{500} and r_{200} . Their r_{200} results were (we used $1.5 \times r_{500}$): 0.57 ± 0.03 (g band), 0.58 ± 0.03 (r band) and 0.58 ± 0.03 (z band) for the $L_{OPT} - L_X$ relation and 1.62 ± 0.10 (g' band), 1.64 ± 0.09 (r' band) and 1.62 ± 0.10 (z' band) for $L_{OPT} - T$ relation. These are in better agreement with our results than Popesso et al. (2004), and demonstrate the importance of the radius used to estimate the L_{OPT} .

5 CONCLUSIONS

We have studied the luminosity functions of 14 Class 1 (C1) XMM-LSS galaxy clusters in three CFHTLS MegaCam bands: g' , r' and z' . The X-ray selected clusters have masses ranging from 0.6 to $19 \times 10^{13} M_\odot$, a redshift range of 0.05 to 0.61 , and ICM temperature range of 0.64 to 4.80 keV. We used colour-magnitude lower and upper cuts to reduce contamination by cluster non-members, and performed background subtraction using the $1^\circ \times 1^\circ$ field of view in which the cluster lies. K-corrected luminosity functions of galaxies within $1.5 \times r_{200}$ were constructed for each cluster and fitted with a Schechter function. Total optical luminosities of the individual clusters were also computed by integrating over the fitted Schechter functions. The individual LFs were also stacked together into 5 different redshift and temperature bins. The main findings are:

- A Schechter function provides a good fit across most of the LF for the majority of clusters in our sample. The value of α range from -1.03 to -2.1 , but no evidence is found for upturns at the faint end of the Schechter function, even in the lowest redshift systems, for which our LFs extend well into the dwarf regime.
- M^* ranges from -19.66 to -24.31 . However, for many (nearly a third) of the clusters' M^* values are not well-constrained.
- The redshift-stacked LFs confirm that α becomes shallower with increasing redshift. The value of α is -1.75 ± 0.02 at low redshift (0.05 - 0.14), flattening to -1.22 ± 0.06 at high redshift (0.43 - 0.61) in the z' band. Similar trends are present in the other two bands.
- α , also steepens significantly from the red (z') to the blue (g') band for clusters at redshift ~ 0.3 . This effect is not present in our local clusters ($z \sim 0$), suggesting reddening of the faint blue galaxies from $z \sim 0.3$ to $z \sim 0$.
- After removing the effects of redshift (correcting for the Malmquist effect), the temperature-stacked LFs do not exhibit any strong evidence for trends of the Schechter parameters with ICM temperature.
- Total optical luminosities for our sample range from 1.0 to $56.3 \times 10^{11} L_\odot$, and correlate strongly with X-ray luminosity. The logarithmic slopes of the $L_{OPT} - L_X$ relation are 0.47 ± 0.07 , 0.43 ± 0.08 and 0.50 ± 0.07 for the g' , r' and z' bands respectively.
- Also, L_{OPT} correlate strongly with the X-ray gas temperature, T . The logarithmic slopes of the $L_{OPT} - T$ relation are

1.57 ± 0.17 , 1.51 ± 0.17 and 1.79 ± 0.12 for the g' , r' and z' bands respectively.

- The slopes of the $L_{OPT} - L_X$ and $L_{OPT} - T$ relations are consistent with the established, non-self-similar, cluster $L_X - T$ relation and constant mass-to-light ratio, except for the z' band value of the $L_{OPT} - T$ relation which is higher than the expected value (1.5) by ~ 0.3 .

- Some of our stacked LFs show dips, but these appear to be artefacts arising where clusters with different faintest magnitude limits are stacked together. We therefore conclude there is no evidence for real dips in the optical LFs of the C1 clusters.

6 ACKNOWLEDGEMENTS

The results presented in this paper are based on observations obtained with MegaPrime/MegaCam, a joint project of CFHT and CEA/DAPNIA, at the Canada-France-Hawaii Telescope (CFHT) which is operated by the National Research Council (NRC) of Canada, the Institut National des Science de l'Univers of the Centre National de la Recherche Scientifique (CNRS) of France, and the University of Hawaii. This work is based in part on data products produced at TERAPIX and the Canadian Astronomy Data Centre as part of the Canada-France-Hawaii Telescope Legacy Survey, a collaborative project of NRC and CNRS.

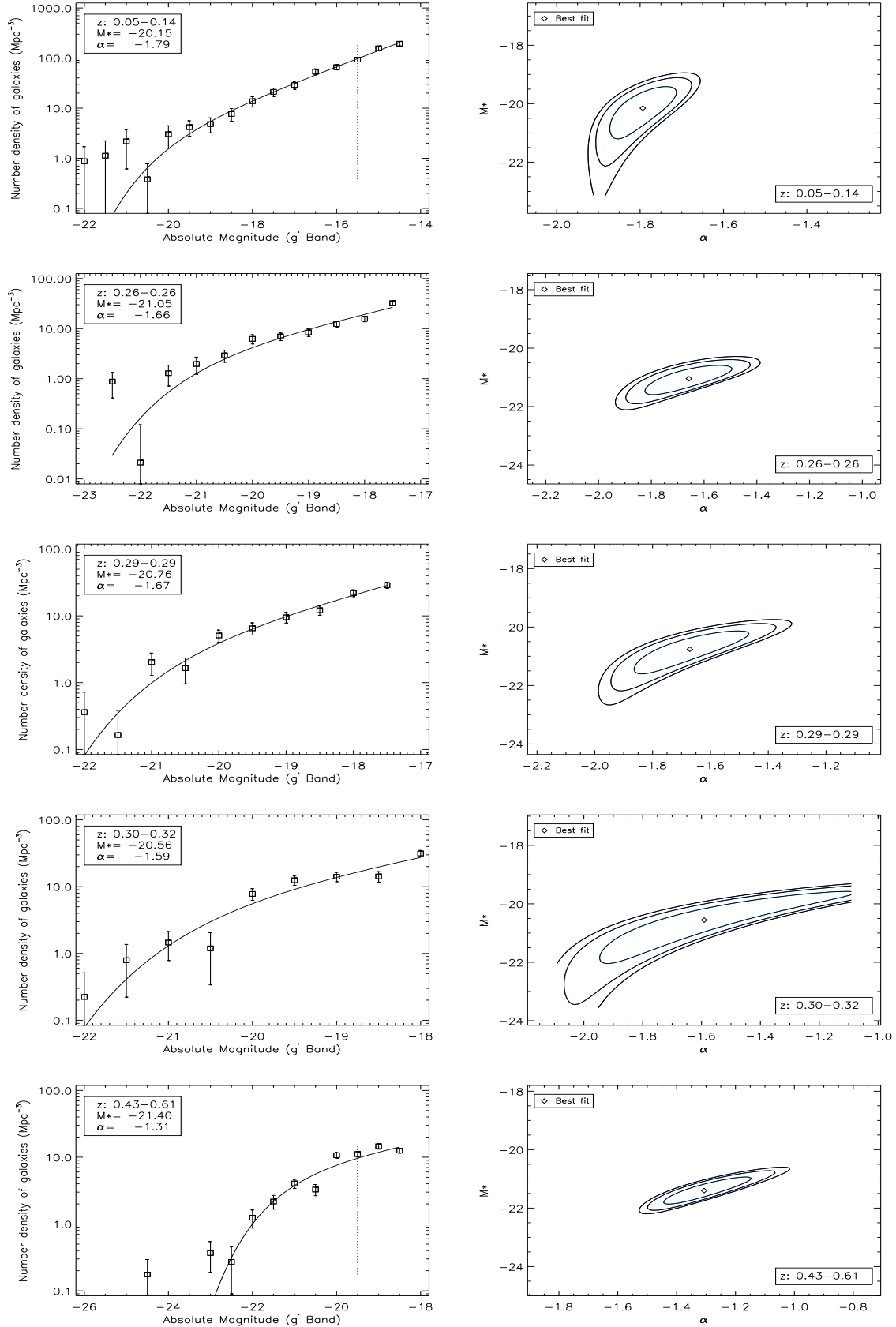


Figure 10. LFs of the stacked clusters for 5 redshift ranges and the associated 1σ , 2σ and 3σ contours for g' band. All stacked clusters contributed to all magnitude bins are at the left side (brighter side) of the vertical dotted line which is at the faintest common magnitude bin of the clusters. Whereas at the right side (fainter side) of it, some clusters did not have data in some magnitude bins because they already reached their faintest magnitude limit.

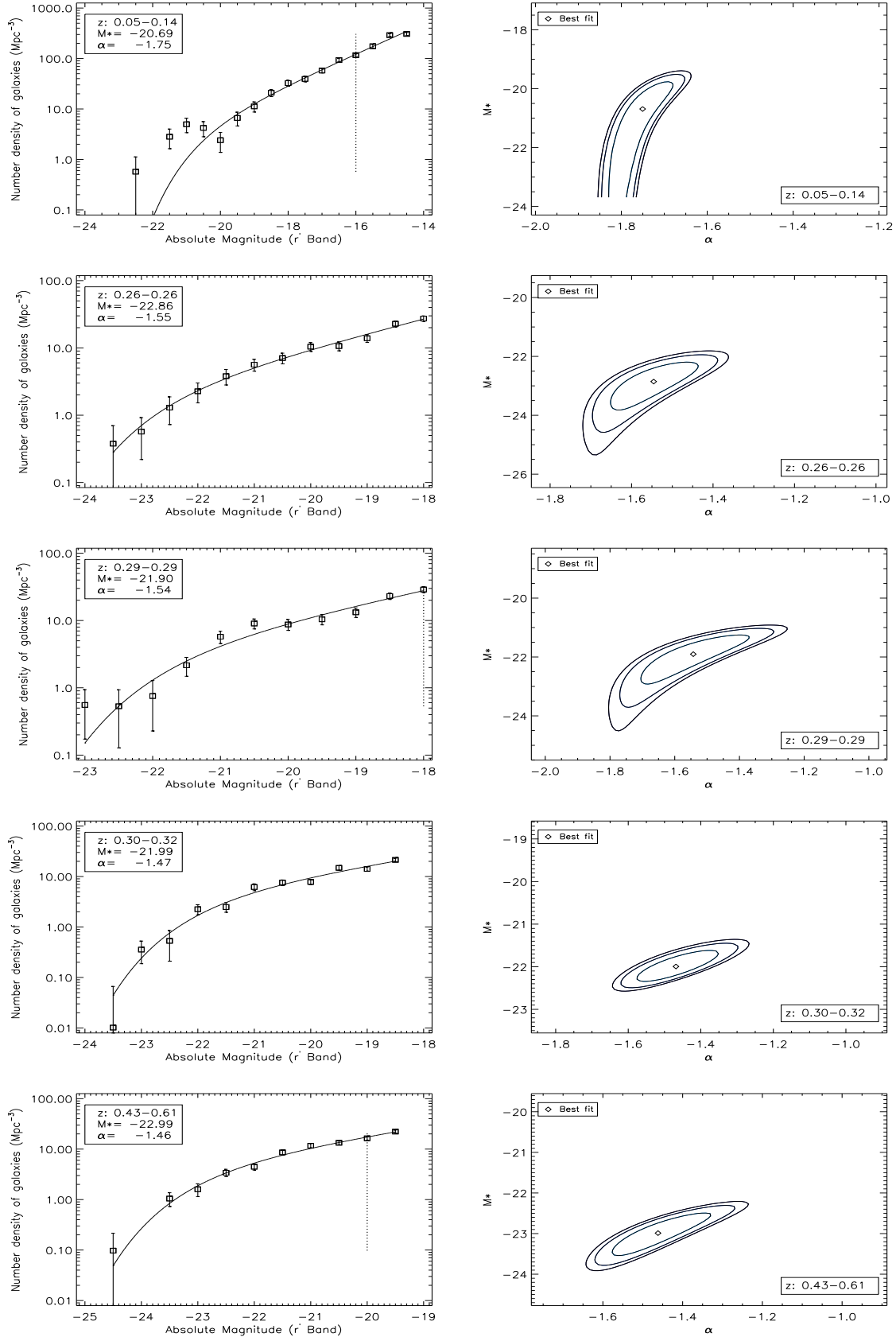


Figure 11. LFs of the stacked clusters for 5 redshift ranges and the associated 1σ , 2σ and 3σ contours for the r' band. The vertical dotted line is at the faintest common magnitude value of all stacked clusters.

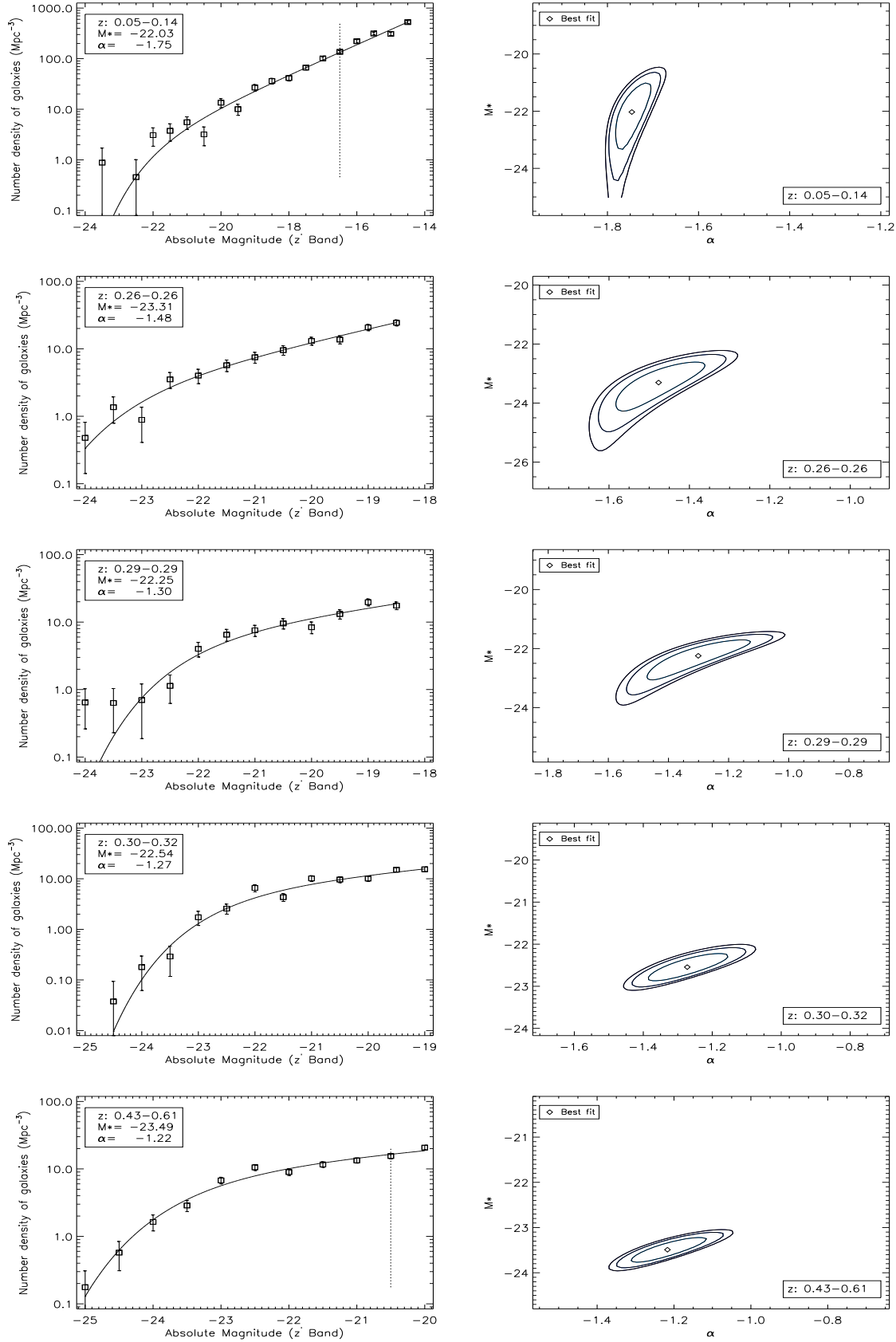


Figure 12. LFs of the stacked clusters for 5 redshift ranges and the associated 1σ , 2σ and 3σ contours for the z' band. The vertical dotted line is at the faintest common magnitude value of all stacked clusters.

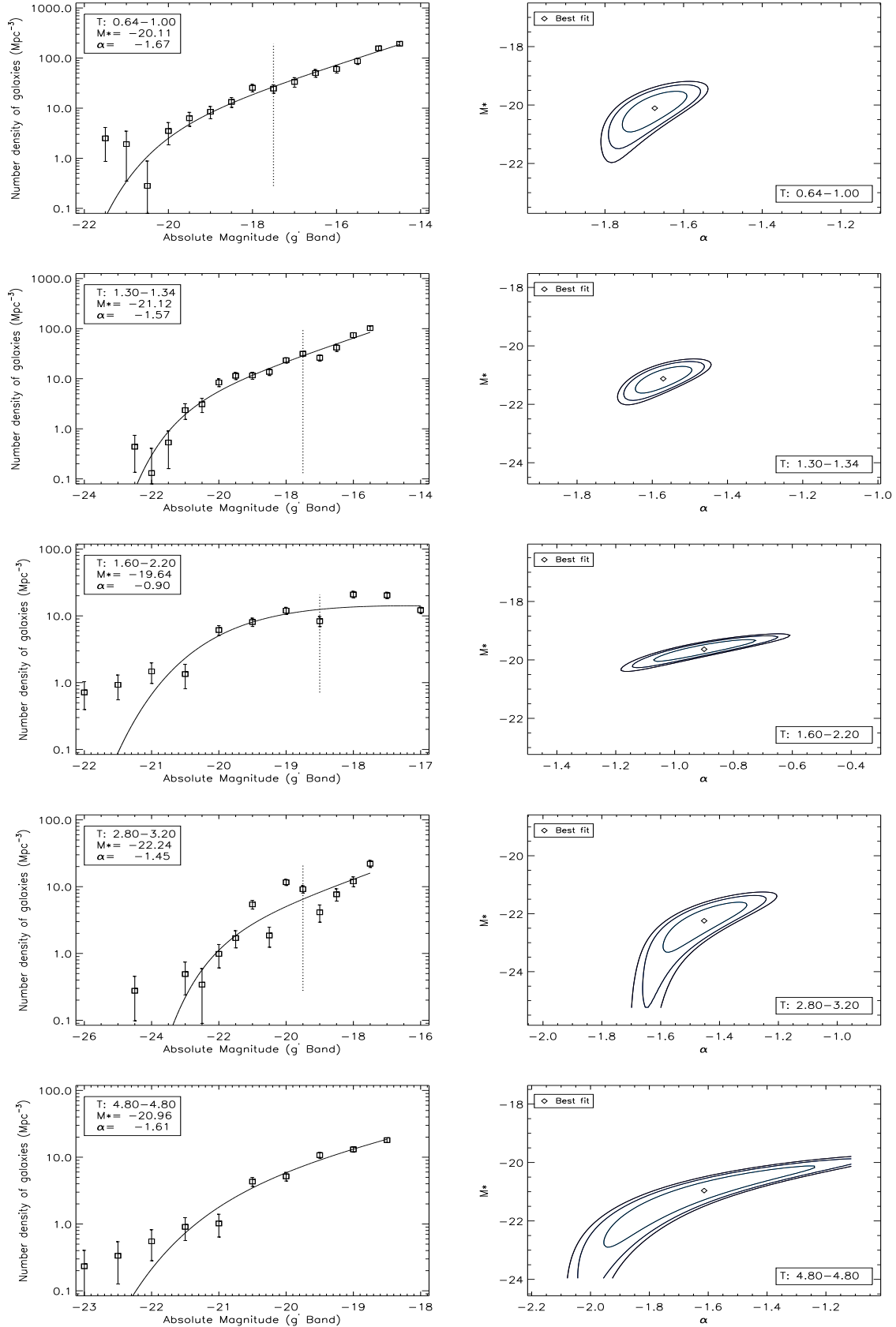


Figure 13. LFs of the stacked clusters for 5 temperature ranges and the associated 1σ , 2σ and 3σ contours for the g' band. The vertical dotted line is at the faintest common magnitude value of all stacked clusters.

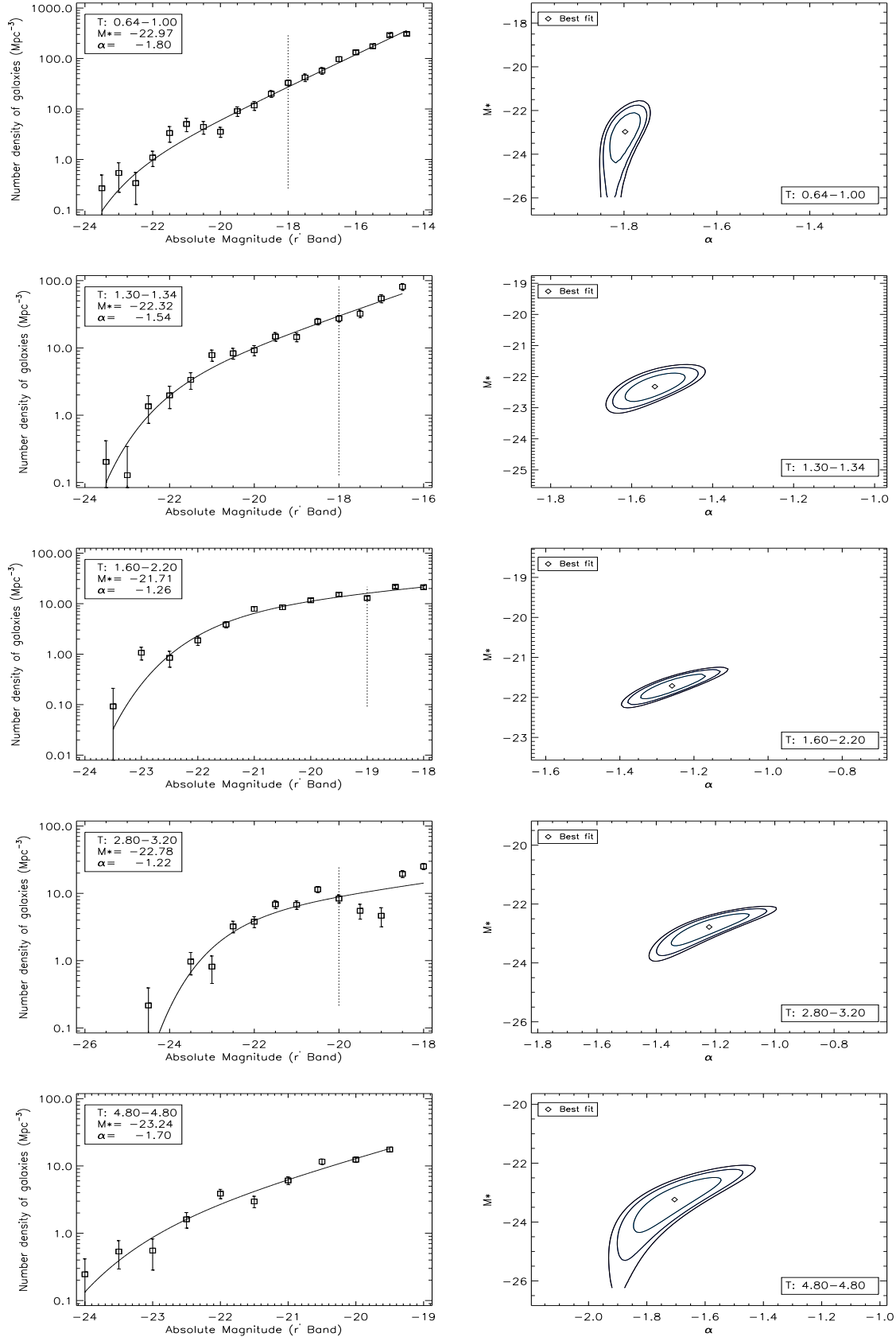


Figure 14. LFs of the stacked clusters for 5 temperature ranges and the associated 1σ , 2σ and 3σ contours for the r' band. The vertical dotted line is at the faintest common magnitude value of all stacked clusters.

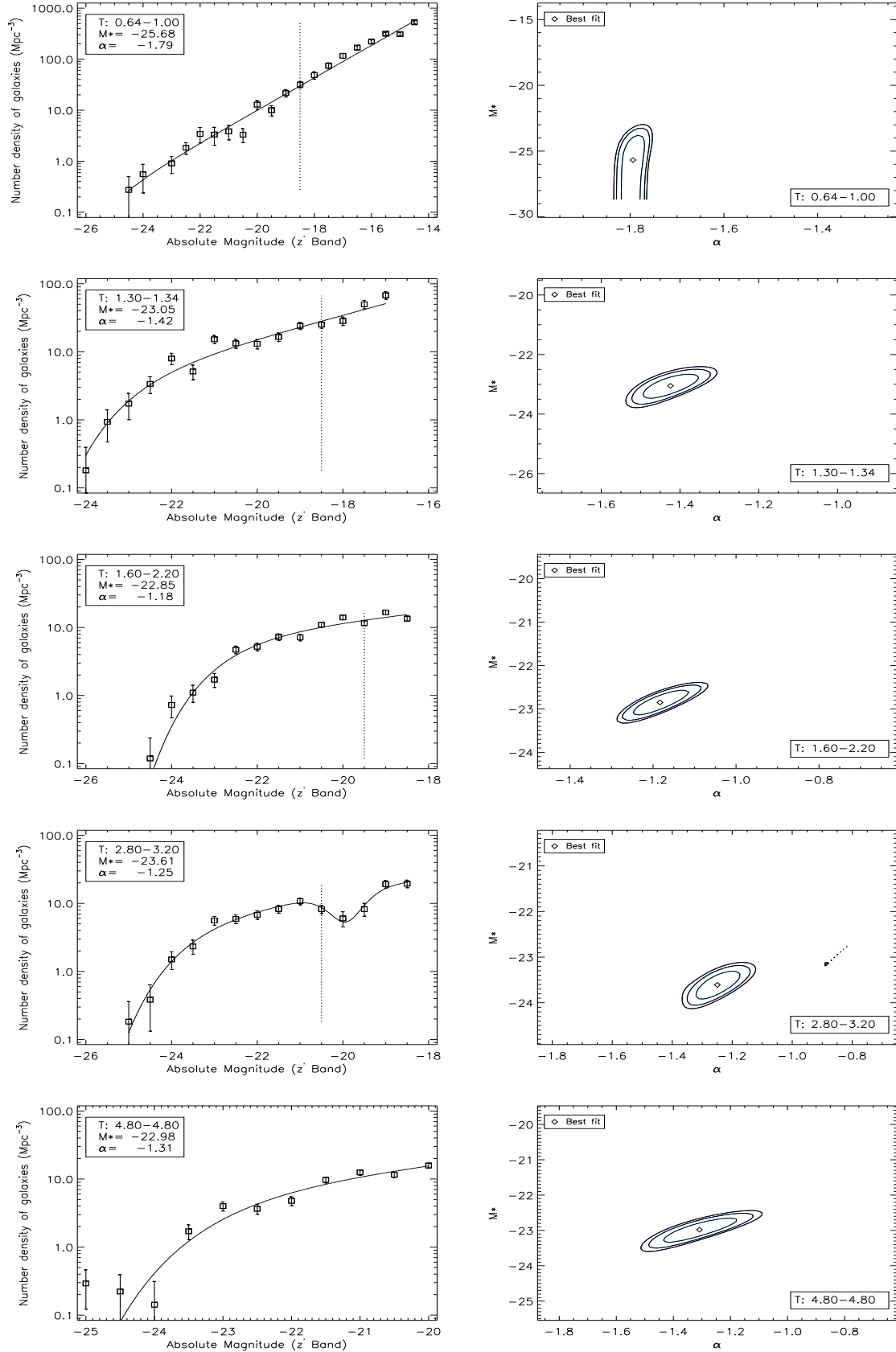


Figure 15. LFs of the stacked clusters for 5 temperature ranges and the associated 1σ , 2σ and 3σ contours for the z' band. The vertical dotted line is at the faintest common magnitude value of all stacked clusters.

REFERENCES

- Adami C., Durret F., Mazure A., Pello R., Picat J. P., West M., Meneuk B., 2007, *A&A*, 462, 411
- Akritas M. G., Bershadsky M. A., 1996, *ApJ*, 470, 706
- Babul A., Rees M. J., 1992, *MNRAS*, 255, 346
- Balogh M. L., Baldry I. K., Nichol R., Miller C., Bower R., Glazebrook K., 2004, *ApJ*, 615, L101
- Bell E. F. et al., 2004, *ApJ*, 608, 752
- Bertin, E., Arnouts, S. 1996, *A&AS*, 117, 393
- Boselli A., Boissier S., Cortese L., Gavazzi G., 2008, *ApJ*, 674, 742
- Boué, G., Adami, C., Durret, F., Mamon, G. A., Cayatte, V. 2008, *A&A*, 479, 335
- Bower R. G., Benson A. J., Malbon R., Helly J. C., Frenk C. S., Baugh C. M., Cole S., Lacey C. G., 2006, *MNRAS*, 370, 645
- Dekel A., Silm J., 1986, *ApJ*, 303, 39
- Durret, F., Adami, C., Lobo, C. 2002, *A&A*, 393, 439
- Frei, Z. & Gunn, J. E. 1994, *AJ*, 108, 1476
- Garilli B., Maccagni D., Andreon S., 1999, *A&A*, 342, 408
- Gilbank, D. G., et al. 2008, *ApJ*, 673, 742
- Girardi M., Manzato P., Mezzetti M., Giuricin G., Limboz F., 2002, *ApJ*, 569, 720
- González R. E., Lares M., Lambas D. G., Valotto C., 2006, *A&A*, 445, 51
- Harsono D., de Propriis R., 2007, *MNRAS*, 380, 1036
- Harsono D., de Propriis R., 2007, *AJ*, 137, 3091
- Hoekstra H. et al., 2006, *ApJ*, 647, 116
- Khochfar S., Silk J., Windhorst R. A., Ryan R. E., 2007, *ApJ*, 668, L115
- King, C. R. & Ellis, R. S. 1985, *ApJ*, 288, 456
- Lin H., Kirshner R. P., Shectman S. A., Landy S. D., Oemler A., Tucker D. L., Schechter P. L., 1996, *ApJ*, 464, 60
- Lisker T., Grebel E. K., Binggeli B., Glatt K., 2007, *ApJ*, 660, 1186
- Liu, C. T., Capak, P., Mobasher, B., et al. 2008, *ApJ*, 672, 198
- Loveday J., Maddox S. J., Efstathiou G., Peterson B. A., 1995, *ApJ*, 442, 457
- Lu Ting, et al. 2009, *MNRAS*, Preprint 2009arXiv0905.3392L
- Marzke R. O., Geller M. J., Huchra J. P., Corwin H. G., 1994, *AJ*, 108, 437
- Miles T. A., Raychaudhury S., Forbes D. A., Goudfrooij P., Ponman T. J., Kozhurina-Platais V., 2004, *MNRAS*, 355, 785
- Moore B., Katz N., Lake G., Dressler A., Oemler A., 1996, *Nat*, 379, 613
- Naab T., Burkert A., 2003, *ApJ*, 597, 893
- Pacaud F. et al., 2006, *MNRAS*, 372, 578
- Pacaud, F., et al. 2007, *MNRAS*, 382, 1289P
- Paolillo M. et al., 2001, *A&A*, 367, 59
- Pierre, M. et al. 2004, *JCAP*, 09, 011
- Popesso P., Bhringer H., Brinkmann J., Voges W., York D. G., 2004, *A&A*, 423, 449
- Popesso P., Bhringer H., Romaniello M., Voges W., 2005a, *A&A*, 433, 415
- Popesso P., Biviano A., Bhringer H., Romaniello M., 2006, *A&A*, 445, 29
- Popesso P., Biviano A., Bhringer H., Romaniello M., Voges W., 2005b, *A&A*, 433, 431
- Rines, K., & Geller, M. J. 2008, *AJ*, 135, 1837
- Robotham A., Wallace C., Phillips S., De Propriis R., 2006, *ApJ*, 652, 1077
- Schechter, P. 1976, *ApJ* 203, 297
- Spergel, D. N., et al. 2007, *ApJ*, 170, 377
- Urquhart, S.A., Willis, J.P., Hoekstra H. and Pierre, M., 'An environmental Butcher-Oemler effect in intermediate redshift X-ray clusters', submitted, 2009, *MNRAS*
- Van Zee L., Barton E. J., Skillman E. D., 2004, *AJ*, 128, 2797
- Wilman D. J. et al., 2005a, *MNRAS*, 358, 88
- Wilman D. J., Balogh M. L., Bower R. G., Mulchaey J. S., Oemler A., Carlberg R. G., Morris S. L., Whitaker R. J., 2005b, *MNRAS*, 358, 71
- Xue Y.-J., Wu X.-P., 2000, *ApJ*, 538, 65
- Yee H. K. C., Hsieh B. C., Lin H., Gladders M. D., 2005, *ApJ*, 629, L77
- Zandivarez A., Martinez H. J., Merchn M. E., 2006, *ApJ*, 650, 137

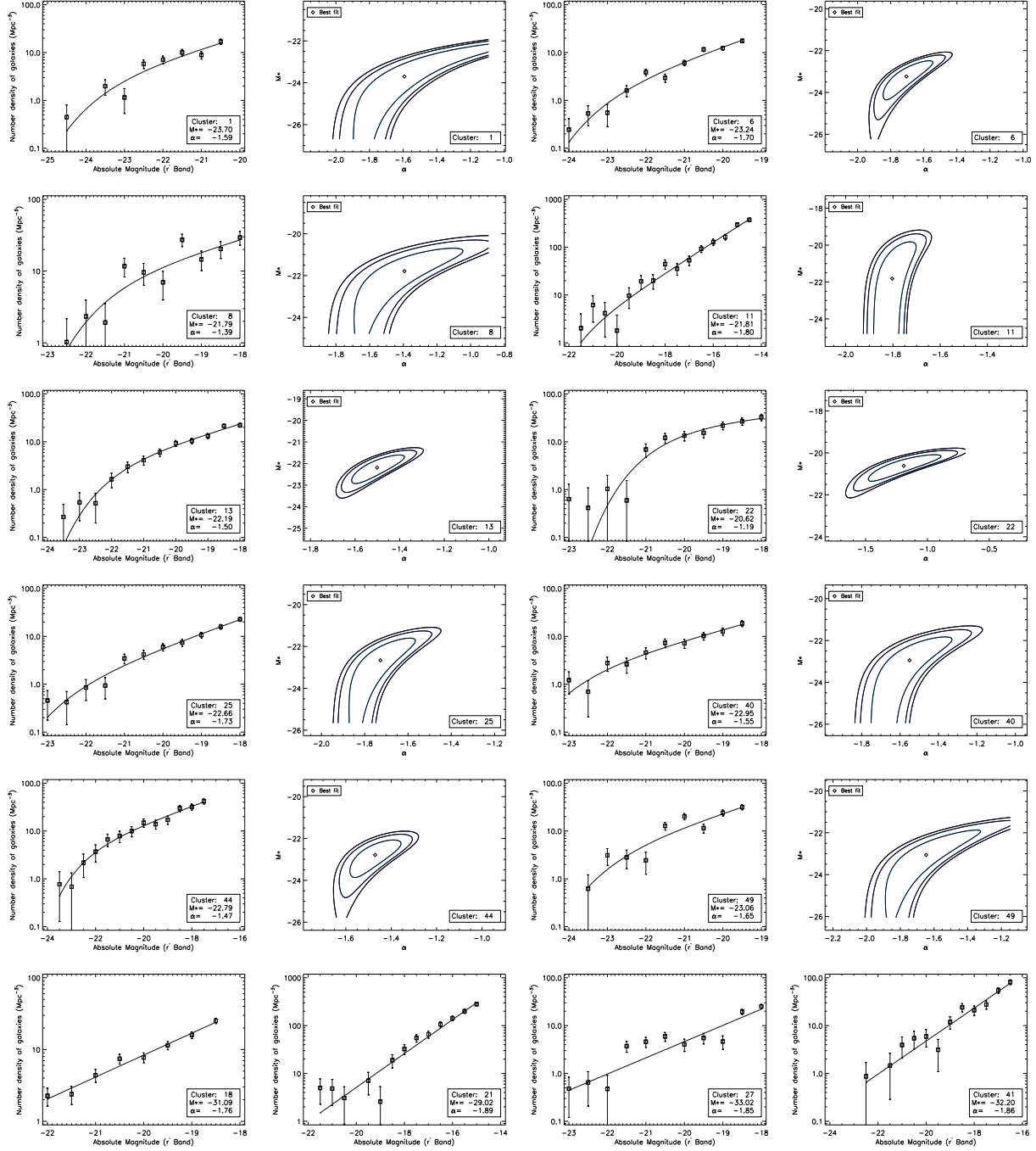


Figure A1. LFs of the 14 individual C1 clusters and contours of the well-fitted clusters for the r' band. Contours plots of the 1σ , 2σ and 3σ confidence levels of α and M^* are placed next to their associated LF. Clusters with failed constrained M^* (and no contours) were placed at the bottom.

APPENDIX A: INDIVIDUAL LUMINOSITY FUNCTIONS OF C1 CLUSTERS IN r' BAND

APPENDIX B: INDIVIDUAL LUMINOSITY FUNCTIONS OF C1 CLUSTERS IN z' BAND

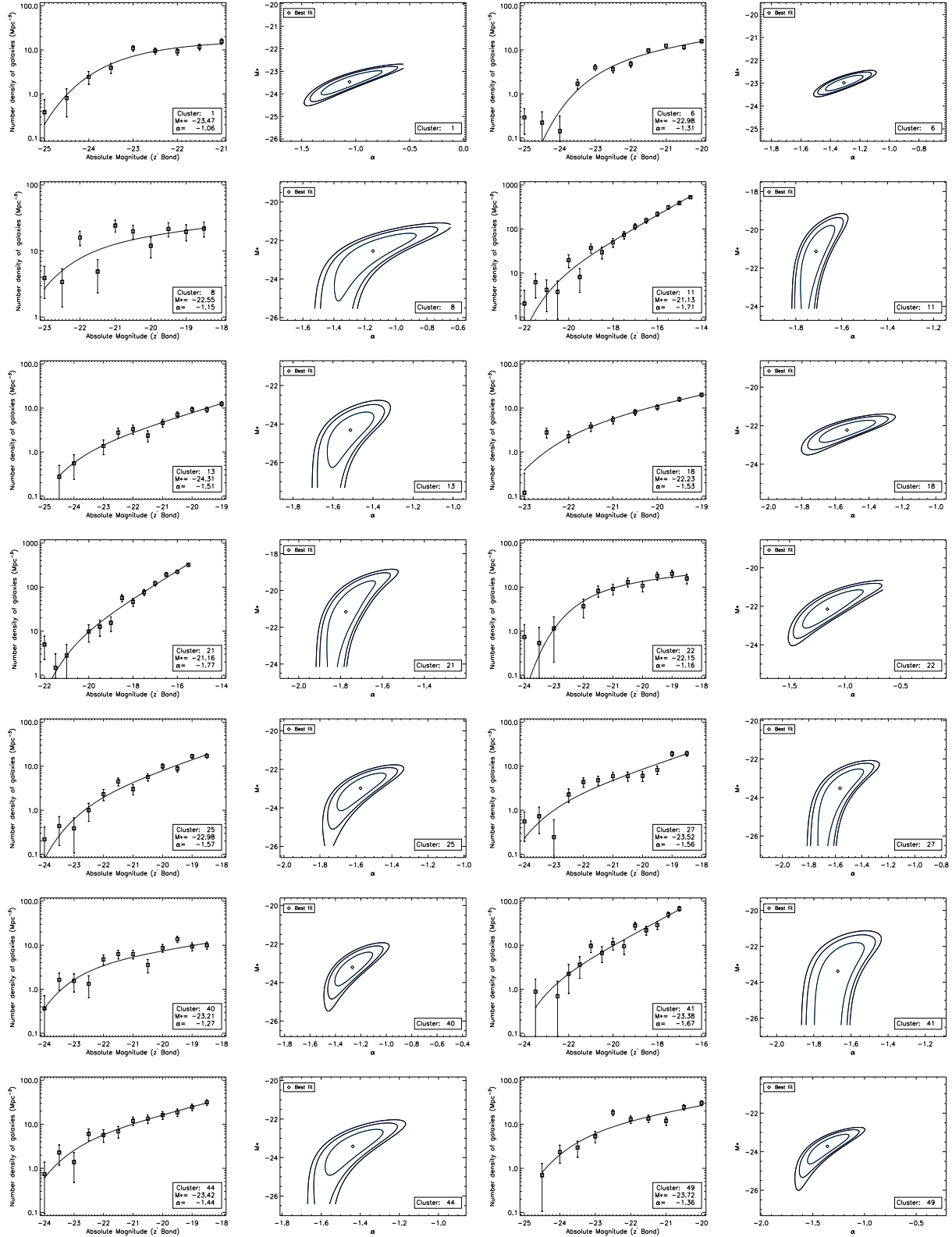


Figure B1. LFs of the 14 individual C1 clusters and the associated 1σ , 2σ and 3σ contours of confidence levels of α and M^* for the well-fitted clusters for the z' band.